2008

The WARPS Survey. VII. The WARPS-II Cluster Catalog

Donald J. Horner
NASA Goddard Space Flight Center

Eric S. Perlman
University of Maryland-Baltimore County

Harald Ebeling
Institute for Astronomy, 2680 Woodlawn Drive, Honolulu, HI

Laurence Jones
University of Birmingham

Caleb A. Scharf
Columbia University

See next page for additional authors

The Astrophysical Journal Supplement Series, 176:374–413, 2008 June

THE WARPS SURVEY. VII. THE WARPS-II CLUSTER CATALOG

Donald J. Horner,[1] Eric S. Perlman,[2,3] Harald Ebeling,[4] Laurence R. Jones,[5]
Caleb A. Scharf,[6] Gary Wegner,[7] Matthew Malkan,[8] and Ben Maughan[9]
Received 2007 November 19; accepted 2007 December 26

ABSTRACT

We present the galaxy cluster catalog from the second, larger phase of the Wide Angle *ROSAT* Pointed Survey (WARPS), an X-ray selected survey for high-redshift galaxy clusters. WARPS is among the largest deep X-ray cluster surveys and is being used to study the properties and evolution of galaxy clusters. The WARPS-II sample contains 125 clusters serendipitously detected in a survey of 301 *ROSAT* PSPC pointed observations and covers a sky area of 56.7 deg^2. Of these 125 clusters, 53 have not been previously reported in the literature. We have nearly complete spectroscopic follow-up of the clusters, which range in redshift from $z = 0.029$ to $z = 0.92$ with a median redshift of $z = 0.29$ and find 59 clusters with $z \geq 0.3$ (29 not previously reported in the literature) and 11 clusters with $z \geq 0.6$ (6 not previously reported). We also define a statistically complete subsample of 102 clusters above a uniform flux limit of 6.5×10^{-14} ergs cm^{-2} s^{-1} (0.5–2.0 keV). Here we provide the cluster catalog and finder charts consisting of X-ray overlays on optical CCD images. We also compare our redshifts, fluxes, and detection methods to other similar published cluster surveys and find no serious issues with our measurements or completeness.

Subject headings: catalogs — galaxies: clusters: general — surveys — X-rays: galaxies: clusters — X-rays: general

1. INTRODUCTION

The Wide-Angle *ROSAT* Pointed Survey (WARPS; Scharf et al. 1997, hereafter Paper I; Jones et al. 1998, hereafter Paper II; Ebeling et al. 2000, hereafter Paper III; Fairley et al. 2000, hereafter Paper IV; Ebeling et al. 2001, hereafter Paper V; Perlman et al. 2002, hereafter Paper VI) is an X-ray–selected survey for high-redshift galaxy clusters based on serendipitous detections in targeted *ROSAT* PSPC observations. The goal of WARPS is to compile a statistically complete, X-ray flux limited sample of galaxy clusters to study the properties and evolution of galaxy clusters. WARPS is designed to detect massive clusters out to $z \approx 1$ and groups of galaxies to somewhat lower redshifts ($z \sim 0.2$–0.3). In total, WARPS covers 70.9 deg^2 and contains a complete sample of 129 clusters above a uniform flux limit of 6.5×10^{-14} ergs cm^{-2} s^{-1}.

In Paper I, we described our source detection methods and survey calibration, including simulations to test and quantify our flux correction methods and sky coverage. In Paper II, we discussed our extensive optical follow-up program to test the validity of our cluster detection techniques and presented the $\log N$–$\log S$ relation for the WARPS-I sample. We found that the number of high-redshift, low-luminosity clusters is consistent with no evolution of the X-ray luminosity function between redshifts of $z \sim 0.4$ and $z = 0$. In Paper III, we reported the discovery and reviewed the properties of WARP J0152.7−1357, an X-ray–luminous, rich cluster of galaxies at a redshift of $z = 0.833$ and discussed the possible effects of highly unrelaxed, merging clusters on conclusions about the evolution of the comoving cluster space density. In Paper IV, we presented a measurement of the cluster X-ray luminosity-temperature (L-T) relation out to high redshift ($z \sim 0.8$) by simultaneously fitting the *ROSAT* PSPC spectra our clusters in redshift and luminosity bins. Our data are consistent with no evolution in the normalization of the L-T relation up to $z \sim 0.8$. In Paper V, we reported the discovery of the galaxy cluster WARP J1226.9+3332. At $z = 0.888$, CL J1226.9+3332 is the most distant X-ray luminous cluster currently known. The mere existence of this system effectively rules out $\Omega_0 = 1$ world models. In Paper VI, we presented a catalog of galaxy clusters detected in the first phase of the WARPS project (WARPS-I), which included data from 86 *ROSAT* Position Sensitive Proportional Counter (PSPC) fields (16.2 deg^2). In addition to the above work, several papers have appeared in the last few years discussing the properties of high-z WARPS clusters in the X-rays. Chief among these are Maughan et al. (2004a), which discussed *Chandra* observations of WARP J1113.1−2615 ($z = 0.72$) and WARP J0152.7−1357 ($z = 0.832$); Maughan et al. (2004a), which discussed *XMM-Newton* observations of WARP J1226.9+3332; Maughan et al. (2004b), which discussed *XMM-Newton* observations of WARP J0046.3+8530 ($z = 0.62$); Maughan et al. (2006a), which discussed *XMM-Newton* and *Chandra* observations of WARP J0152.7−1357; and Maughan et al. (2006b), which discussed cluster X-ray scaling relations in $z > 0.6$ WARPS clusters. Following this paper, the evolution of the X-ray luminosity function will be discussed in L. R. Jones et al. (2008, in preparation).

After the completion of WARPS-I, we embarked on a larger survey (WARPS-II) using 301 PSPC fields (56.7 deg^2). In this paper, we present the catalog of galaxy clusters found during the WARPS-II survey. In general, the two phases of the survey had identical source selection and identification procedures. However, they do have some small differences. WARPS-I was partly a test of the ability of our algorithm to correctly detected extended sources like clusters of galaxies; consequently, we undertook an extensive

[1] NASA Goddard Space Flight Center, Code 660.1, Greenbelt, MD 20771.
[2] Department of Physics, University of Maryland-Baltimore County, 1000 Hilltop Circle, Baltimore, MD 21250.
[3] Current Address: Physics and Space Sciences Department, Florida Institute of Technology, 150 West University Boulevard, Melbourne, FL 32901.
[4] Institute for Astronomy, 2680 Woodlawn Drive, Honolulu, HI 96822.
[5] School of Physics and Astronomy, University of Birmingham, Birmingham B15 2TT, England, UK.
[6] Columbia Astrophysics Laboratory, Columbia University, Mail Code 5247, 550 West 120th Street, New York, NY 10027.
[7] Department of Physics and Astronomy, Dartmouth College, 6127 Wilder Laboratory, Hanover, NH 03755.
[8] Department of Physics and Astronomy, University of California, Los Angeles, CA 90024.
[9] Current Address: University of Bristol, H. H. Wills Physics Laboratory, Tyndall Avenue, Bristol BS8 1TL, England, UK.

optical follow-up campaign of imaging and spectroscopy on many extended, possibly extended, and even some point sources. We found that we successfully detected clusters as extended sources, even at high redshifts, and so our optical follow-up for WARPS-II was less extensive but more efficient.

In § 2 we describe briefly the survey methods and source identification process. In § 3 we describe the statistically complete, flux-limited WARPS-II sample of clusters of galaxies and also comment on individual clusters. Several similar surveys to WARPS (i.e., based on *ROSAT* serendipitous observations) are the *ROSAT* Distant Cluster Survey (RDCS; Rosati et al. 1998), the CfA 160 deg^2 (160SD) survey (Vikhlinin et al. 1998; Mullis et al. 2003), the Serendipitous High-Redshift Archival *ROSAT* Cluster Survey (BSHARC, Romer et al. 2000; SSHARC, Burke et al. 2003), and the *ROSAT* International X-ray/Optical Survey (RIXOS; Mason et al. 2000). We will reference these surveys throughout in this paper and make a detailed comparison in § 4. Finally, we discuss and summarize our results in § 5.

We assume that groups and clusters of galaxies form a continuous population, referred to simply as "clusters," and do not further distinguish between groups and clusters of galaxies. We assume $q_0 = 0.5$ and $H_0 = 50$ km s^{-1} Mpc^{-1} when calculating distance dependent quantities to maintain consistency with previous WARPS papers, but also give luminosity values in a more fashionable $\Omega_m = 0.3,\ \Omega_\Lambda = 0.7,\ H_0 = 70$ km s^{-1} Mpc^{-1} cosmology. Similarly, we use the 0.5–2.0 keV *ROSAT* PSPC band when quoting count rates, fluxes, and luminosities unless otherwise noted. In this paper, we only list the galaxy clusters, but the complete catalog of source detections, identifications, finder charts, and other information can be found on our WARPS Web site.[10]

2. SURVEY METHODS

Our methods have been discussed extensively in our previous papers, especially Paper VI about the WARPS-I sample, so here we only highlight certain aspects.

2.1. *Field Selection*

The WARPS-II cluster sample was compiled from nonoverlapping, nonboron filter *ROSAT* PSPC pointed observations with exposure times in excess of 8 ks. We included only fields at $|b| > 20^\circ$ to avoid obscuration by the Galactic equator. We excluded fields below $\delta \leq -30^\circ$ or in the right ascension range $2^h < \alpha < 8^h$ due to constraints from our optical follow-up program based primarily on telescopes in Hawaii and to avoid the Galactic plane. To minimize biases and source confusion, we further excluded observations pointed at known galaxy clusters and observations containing large nearby galaxies, bright stars, star clusters, or Galactic molecular clouds. We also excluded fields with high Galactic column density or high background level (>0.7 counts s^{-1}). The final WARPS-II sample contains 301 fields covering a total sky area of 56.7 deg^2. Table 1 lists the sequence number, exposure time, right ascension, and declination of the field center, and target name for each field in the WARPS-II sample. Figure 1 shows the distribution of the target fields on the sky.

2.2. *X-Ray Source Detection*

We searched for sources in a 3′–15′ annulus around the center of each *ROSAT* field. The inner boundary excluded the target of the observation, while the outer boundary ensured that the point-spread function (PSF) had a full width at half-maximum (FWHM) of less than 45″ and avoided strong shading by the PSPC window support structure. We used the 0.5–2.0 keV band for source detection and flux measurement to minimize both the size of the PSF and the background relative to typical cluster spectra. This energy band is also nearly optimal for detecting hot massive clusters at high redshift (Scharf 2002). We employed the Voronoi Tessellation and Percolation (VTP; Ebeling 1993; Ebeling & Wiedenmann 1993) algorithm to detect both extended and pointlike X-ray sources. VTP is a general method for detecting non-Poissonian structure in a two-dimensional event distribution. See Papers I and II for more details.

We ran VTP five times on each field using different surface brightness thresholds in order to distinguish real, single sources from those composed of blends of several sources (pointlike or extended). We then selected the optimal surface brightness threshold for each field by visually inspecting the VTP source photon distribution for each of the five thresholds. This procedure not only allowed us to separate sources blended together at low percolation thresholds, but also permitted us to identify and merge complex extended sources split into several fainter sources at high percolation thresholds. We estimated the total count rate for each source, which accounts for undetected flux below the limiting X-ray isophote, from the detected count rate by extrapolating the surface brightness using a King profile with $\beta = 2/3$ to infinite radius (extrapolating to the virial radius would give count rates about 10% lower). The normalization and core radius were estimated from the PSPC data.

To characterize the extent of a source, we also estimated the total count rate assuming the source surface brightness followed a pointlike profile rather than King profile. We classify an object as extended if its extent parameter $f_{\rm ext}$, defined as the ratio of the King-to-point count rates, lies above 1.2, and "marginally extended" if $1.1 < f_{\rm ext} < 1.2$. This extent criterion was empirically determined from both simulation results (see Paper I) and survey data itself. For the WARPS-I sample, we found that the extent parameter was a good judge of distinguishing clusters candidates from point sources. We followed up many pointlike detections as well as extended sources (see Paper VI). Only one cluster (out of 22) in the WARPS-I statistically complete sample was found to be pointlike, with $f_{\rm ext} < 1.1$ (WARP J2302.8+0843 at $z = 0.722$), and the cluster fraction was found to increase markedly at higher values of f: 11% of sources with $1.1 < f_{\rm ext} < 1.2$ were found to be clusters, a fraction that increases to 47% of sources with $f_{\rm ext} > 1.2$. Therefore, for WARPS-II we only follow up extended and possibly extended sources, i.e., those with $f_{\rm ext} > 1.1$.

2.3. *Optical Follow-up Program*

Optical follow-up of X-ray detections is necessary to confirm the existence of a cluster and obtain its redshift. Our optical follow-up program for WARPS-II is similar to that for WARPS-I discussed in detail in Paper VI. Optical images (usually *R*- or *I*-band CCD images, although for low-redshift clusters Digitized Sky Survey images occasionally sufficed) were obtained of cluster candidates, and those which showed an excess of galaxies within the X-ray contours were selected for spectroscopic follow-up to confirm the cluster and obtain its redshift. We identify an X-ray source as a cluster if at least two galaxies in the case of two or three spectra of good signal-to-noise ratio (SNR) or at least three galaxies in the case of four or more spectra have very similar redshifts, and if it can be reliably determined that the X-rays were not emitted by an AGN, star, or other point source (some blends are present; see § 3.2). We performed no near-infrared imaging follow-up, unlike the RDCS, which explains why WARPS contains only

[10] See http://asd.gsfc.nasa.gov/Donald.Horner/warps/index.html.

TABLE 1
ROSAT PSPC Pointings Used in WARPS-II

Sequence	Exposure Time (ks)	α (deg)	δ (deg)	Target Name
RP100308N00	21.5	199.10	29.10	WFC MAIN GRID HZ
RP100366N00	17.1	177.27	14.57	WFC UV LEAK BETA
RP100376N00	17.0	19.65	−22.92	WFC FOCUS CHECK
RP100378N00	50.4	270.00	66.56	WFC BACKGROUND N
RP100578N00	10.3	348.09	10.78	WFC SPEC/FLUX BP
RP150046N00	11.5	214.94	54.39	OQ 530
RP170001N00	27.2	225.53	66.21	CALIBRATION SOUR
RP170154N00	36.7	247.39	78.08	CALIBRATION SOUR
RP200076	26.5	154.91	19.87	AD LEO
RP200091N00	31.8	174.14	29.80	GD140
RP200127	16.7	165.85	36.04	GL411
RP200208N00	25.4	24.18	−18.37	UV CETI
RP200213N00	21.4	168.53	20.52	DELTA LEO
RP200322N00	23.2	351.34	23.40	HR 8905
RP200329N00	25.6	217.18	33.18	LHS 2924
RP200403N00	9.1	155.58	41.50	UMA
RP200453N00	15.7	126.72	26.63	DX CNC
RP200468N00	8.5	25.84	4.33	GLIESE 70
RP200470N00	8.5	141.90	−8.66	HYA
RP200473N00	8.8	124.95	37.52	GD 90
RP200561N00	8.6	138.99	53.42	EG 250
RP200943N00	9.8	165.21	39.21	49 UMA
RP201006	9.3	235.52	−19.47	LHS 54
RP201020N00	14.7	161.34	45.57	TX UMA
RP201032	9.9	241.53	23.61	HR 5988
RP201066N00	18.9	269.15	51.49	GAMMA DRACONIS
RP201136N00	8.1	250.32	31.60	HR 6212
RP201367M01	50.7	181.11	−3.67	PG 1159−035
RP201382N00	37.0	137.38	54.40	XY UMA
RP201446N00	24.4	250.23	53.69	GD 356
RP201476N00	9.3	243.57	−19.00	SMOKE RINGS
RP201488N00	13.9	17.45	19.66	HD 6903
RP300016	26.7	7.52	26.29	PG 0027+260
RP300034N00	15.0	187.53	69.20	4 DRA
RP300067A01	18.0	274.06	49.87	AM HER
RP300103N00	13.2	271.88	45.86	DQ HER
RP300120N00	8.5	343.82	−3.18	AO PSC
RP300121N00	8.9	327.99	14.11	S193
RP300137N00	9.3	164.24	49.69	CY UMA
RP300181	45.9	250.42	36.46	NGC 6205
RP300194N00	10.2	188.73	37.63	AM CVN
RP300285N00	19.7	205.26	51.90	UX UMA
RP300314N00	14.7	285.90	68.55	H1907+690
RP300333A01	14.6	205.54	28.38	NGC 5272
RP400020N00	10.8	129.70	36.52	GBS 0839+37
RP400043N00	14.6	272.94	31.41	GRB 790325B
RP400059N00	8.9	148.29	7.93	PSR 0950+08
RP400081N00	8.8	322.49	12.17	2127+11
RP400374N00	22.1	254.46	35.34	HER X-1
RP500157N00	20.2	165.72	60.89	G290.1−0.8
RP600005N00	22.8	28.25	−13.74	NGC 720
RP600008N00	8.5	186.36	18.19	NGC 4382
RP600009N00	14.8	186.11	7.32	NGC 4365
RP600017N00	14.1	190.93	11.56	NGC 4649
RP600051A01	9.1	154.57	41.42	NGC 3184
RP600129A00	19.5	190.53	32.54	NGC 4631
RP600130N00	22.7	183.77	33.20	NGC 4203
RP600143N00	8.8	352.14	14.75	PEGASUS DWARF IR
RP600156N00	9.1	159.69	53.50	NGC 3310
RP600158N00	24.0	202.47	47.20	N5194/N5195
RP600159A00	9.5	11.79	−20.76	NGC 247
RP600162N00	12.0	188.48	26.27	NGC 4565
RP600165N00	16.8	143.51	55.24	I ZW 18
RP600166N00	12.7	184.79	3.86	MK 49
RP600169N00	16.3	123.31	45.99	MK 86

TABLE 1—*Continued*

Sequence	Exposure Time (ks)	α (deg)	δ (deg)	Target Name
RP600174N00	18.5	150.78	−26.16	NGC 3109
RP600175N00	15.8	332.28	−27.81	22062−2803
RP600179N00	9.3	184.38	37.81	NGC 4244
RP600189N00	13.3	184.18	69.47	NGC 4236
RP600207N00	17.3	143.97	61.35	UGC 5101
RP600235N00	17.4	335.20	−24.68	NGC 7252
RP600236N00	22.5	175.80	55.07	NGC 3921
RP600237N00	9.2	191.53	30.73	NGC 4676
RP600242A01	24.8	186.93	1.60	GIOVANELLI-HAYNE
RP600258N00	10.6	190.00	−11.62	NGC 4594
RP600261N00	20.6	162.46	33.00	ARP 270
RP600262A02	45.3	192.15	−5.80	NGC 4697
RP600270N00	34.8	207.31	60.19	NGC 5322
RP600518N00	21.4	188.51	7.70	NGC 4526
RP600532N00	16.8	191.29	0.46	NGC 4666
RP600537N00	17.5	169.73	13.09	NGC 3623
RP600538A01	9.5	185.30	18.38	NGC 4293
RP600541N00	13.1	21.38	1.76	NGC 533
RP600595A02	17.4	188.99	27.96	NGC 4559
RP600625N00	14.1	182.89	39.02	MS 1209+3917
RP700010N00	13.9	170.07	13.59	NGC 3628
RP700050N00	8.5	155.48	21.99	3C 241
RP700055	58.5	179.48	55.45	NGC 3998
RP700056N00	9.3	189.43	11.82	NGC 4579
RP700058N00	11.3	280.53	79.77	3C 390.3
RP700072N00	8.7	144.85	83.26	3C 220.3
RP700073	48.1	194.24	47.34	3C 280
RP700120	19.1	136.38	34.13	B2 0902+343
RP700121	8.4	15.57	−27.33	Q0059−2735
RP700123N00	8.1	255.35	51.82	Q1700+5153
RP700142N00	8.4	291.95	73.97	S51928+73
RP700211N00	18.9	140.40	62.26	S4 0917+62
RP700221N00	21.6	184.46	30.12	B2 1215+30
RP700228N00	24.3	169.79	21.32	1116+215
RP700232N00	25.7	181.18	27.90	1202+281
RP700246N00	9.3	248.62	70.53	1634+706
RP700248N00	24.8	213.45	44.00	1411+442
RP700255N00	8.4	247.58	37.32	1628+374
RP700258N00	8.2	121.13	65.00	IRAS 07598+6508
RP700263N00	13.9	152.56	52.75	SURVEY FIELD 3
RP700264N00	14.8	152.57	53.75	SURVEY FIELD 2
RP700265A01	20.1	152.56	51.75	SURVEY FIELD 4
RP700275N00	24.5	13.02	−29.09	SGP2
RP700277N00	36.7	182.63	39.41	NGC 4151
RP700283N00	71.8	203.65	37.91	DEEP SURVEY
RP700319N00	18.8	150.49	55.68	NGC 3079
RP700329A01	22.1	137.39	42.90	3C 216
RP700330N00	9.8	224.78	71.67	3C 309.1
RP700355N00	23.5	189.10	0.91	QNY1
RP700358N00	14.2	169.57	7.77	1115+080
RP700376N00	12.2	197.90	−5.88	Q1309−056
RP700379N00	8.4	148.48	−5.07	BR I 0952−01
RP700384N00	10.0	160.69	12.06	1040+123
RP700387N00	17.1	145.27	38.90	0937+391
RP700388N00	8.3	186.41	24.98	1223+252
RP700392N00	11.4	209.01	18.37	MRK 463
RP700424A01	19.3	14.45	30.35	NGC 315
RP700436N00	21.5	134.67	14.15	3C 212
RP700461N00	13.4	157.98	−14.28	HE 1029−1401
RP700467N00	36.9	0.85	−26.06	Q0000−26
RP700473N00	9.8	204.57	48.28	MKN 266
RP700499N00	8.7	171.40	54.38	MKN 40
RP700530N00	9.8	181.35	−7.71	BR1202−07
RP700540N00	19.2	156.14	47.15	10214+4724
RP700546N00	12.2	132.08	37.67	E0845+378
RP700547N00	12.2	309.38	−22.71	E2034−228

TABLE 1—*Continued*

Sequence	Exposure Time (ks)	α (deg)	δ (deg)	Target Name
RP700557M01	20.8	181.70	44.35	NGC 4051
RP700803N00	8.4	200.96	65.70	PG 1322+659
RP700833N00	10.9	177.58	24.30	1147+245
RP700855N00	16.2	168.66	40.62	1111+408
RP700864A01	19.3	185.14	33.72	3C 270.1
RP700865	10.7	214.78	6.48	3C 298
RP700872N00	13.1	166.70	72.57	NGC 3516
RP700873N00	24.7	338.94	−26.05	NGC 7314
RP700875N00	34.8	257.18	71.13	DRACO SURVEY FIE
RP700882N00	15.8	140.56	74.99	0917
RP700887N00	18.6	133.29	13.88	0850+140
RP700897	10.2	234.69	−3.38	CGCG 022−021
RP700922N00	20.7	206.18	55.89	MKN 273
RP700996N00	19.6	155.88	19.86	NGC 3227
RP700999A02	16.4	161.60	−0.03	BJS 855
RP701001	10.0	231.10	9.97	1522+101
RP701025N00	11.3	314.02	−19.94	2053−201
RP701214N00	12.5	147.44	73.24	4C 73.08
RP701367N00	14.3	147.70	39.45	PG 0947+396
RP701368N00	8.1	162.93	33.99	PG 1048+342
RP701375N00	14.8	134.54	27.85	3C 210
RP701390N00	10.4	333.82	−29.99	Q2212−299
RP701407N00	15.6	24.99	1.53	0137+012
RP701409N00	17.0	250.95	17.26	1641+173
RP701410N00	13.9	296.23	77.10	Q1946+77
RP701424N00	9.6	208.26	69.31	MKN 279
RP701433N00	8.4	12.67	−9.48	PKS 0048−097
RP701439N00	15.4	256.17	60.74	3C 351
RP900009	73.7	132.30	44.84	LYNX.3A
RP900211N00	27.1	256.27	59.62	HI−FILAMENT
RP900213N00	16.6	152.57	54.75	SURVEY FIELD 4
RP900214N00	15.7	152.55	50.75	SURVEY FIELD 5
RP900215N00	18.8	152.58	55.75	SURVEY FIELD 6
RP900239N00	19.2	133.77	17.08	VLB
RP900244N00	10.0	205.17	−19.88	A36
RP900323N00	10.6	347.17	−27.43	G026−67
RP900326N00	8.9	19.01	−3.57	G138−66
RP900327A01	30.9	136.72	33.67	ZELDOVICH PANCA
RP900329N00	10.1	164.55	64.49	UMA5
RP900331N00	9.0	164.38	62.27	UMA7
RP900332A01	9.3	167.58	64.54	UMA8
RP900336N00	10.3	173.84	59.72	UMA12
RP900349N00	10.4	127.18	9.33	G213+26
RP900405N00	8.7	205.51	40.54	SURVEY POSN. 17
RP900496A01	22.7	13.75	−28.33	SGP3
WP180014N00	16.1	266.56	62.45	TOO Q1746+624
WP180019N00	13.5	166.00	−18.00	TOO HE 1104−18AB
WP180026N00	9.9	278.48	51.72	TOO ORFEUS BY DR
WP200654	35.4	130.32	64.38	PI**1 UMA
WP200681	8.9	17.15	−10.18	ETA CET
WP200721	47.5	248.60	57.15	CM DRA
WP201077	9.1	6.92	5.06	PC 0025+0447
WP201216N00	9.6	269.06	37.25	THETA HER
WP201219	9.3	165.05	−14.08	HR 4289
WP201222N00	8.4	326.13	17.35	9 PEG
WP201223N00	8.9	144.27	81.33	HD 81817
WP201227N00	8.6	246.00	61.51	ETA DRA
WP201241	9.4	281.75	55.64	RX J1846.9+5538.
WP201243N00	18.1	159.27	0.01	PG 1034+001
WP201282N00	12.5	344.37	20.77	51 PEG
WP201325	15.6	29.45	37.68	NGC 752
WP201326N00	15.8	132.85	11.83	M67
WP201327N00	17.6	11.10	85.33	NGC 188
WP201514N00	18.8	193.89	25.89	LOTR 5
WP201516N00	9.0	258.76	36.81	PI HER
WP201536N00	12.3	225.49	40.39	BETA BOO

TABLE 1—*Continued*

Sequence	Exposure Time (ks)	α (deg)	δ (deg)	Target Name
WP201552N00.....	18.0	342.50	24.60	MU PEG
WP201558N00.....	19.0	233.67	26.72	HR5793
WP201723N00.....	13.2	339.63	−15.31	GJ 866
WP201753A01.....	14.5	322.76	23.34	RE 2131+23
WP201763N00.....	19.4	309.32	75.59	VW CEP (PHASE 0.
WP201766N00.....	8.1	258.49	16.35	AK HER
WP300135.....	10.1	342.42	−27.11	TY PSA
WP300158.....	14.0	161.81	54.31	EK UMA
WP300222N00.....	10.8	151.90	−20.28	RX J1007.6−2017
WP300234A01.....	12.0	162.90	54.08	EK UMA
WP300287N00.....	16.7	176.71	28.74	RE 1149+28
WP300291N00.....	44.0	165.67	25.08	ST LMI
WP300367N00.....	13.4	176.28	72.35	DO DRA
WP300387N00.....	16.6	258.23	33.52	V795 HER
WP300394N00.....	12.0	196.97	53.86	RE 1307+535
WP400141.....	9.0	145.93	16.52	PSR 0940+16
WP400388N00.....	9.4	254.29	−4.10	NGC6254
WP500308N00.....	8.7	311.76	−0.02	G311.4−0.4
WP600178.....	14.5	150.50	−8.16	09595−0755
WP600190.....	18.2	228.98	56.32	NGC 5907
WP600277.....	9.0	186.45	33.55	NGC 4395
WP600278N00.....	8.8	159.77	41.69	NGC 3319
WP600280N00.....	10.5	161.64	63.24	NGC 3359
WP600415A01.....	10.5	189.09	25.98	NGC 4565
WP600416.....	18.1	190.99	32.17	NGC 4656
WP600417A01.....	10.3	184.29	7.19	NGC 4235
WP600420.....	11.7	175.54	10.28	11395+1033
WP600421N00.....	11.1	243.84	68.39	16155+6831
WP600424N00.....	9.3	267.95	23.07	NGC 6482
WP600431N00.....	11.6	124.82	70.71	HOL II
WP600437A01.....	18.0	189.20	13.17	NGC 4569
WP600450.....	10.5	190.93	16.40	3C 275.1/NGC 465
WP600458N00.....	18.1	202.40	58.42	NGC 5204
WP600468A02.....	16.9	180.48	−18.88	NGC 4038/9
WP600544N00.....	18.9	348.42	14.02	MKN 316
WP600546N00.....	25.7	184.74	47.31	NGC 4258
WP600570N00.....	10.4	172.01	78.99	VII ZW 403
WP600575N00.....	16.2	154.98	45.55	NGC 3198
WP600585N00.....	10.2	228.85	55.52	NGC 5905
WP600587N00.....	23.4	186.62	9.02	NGC 4410
WP600588N00.....	17.3	241.30	20.54	MRK 297
WP600589N00.....	8.6	154.23	73.38	NGC 3147
WP600624N00.....	8.4	155.55	51.40	MS 1019+5139
WP700216.....	13.0	197.62	32.35	B2 1308+32
WP700262.....	10.3	141.30	52.29	MKN 110
WP700498.....	9.5	301.84	77.88	S5 2007+77
WP700506.....	8.8	187.10	31.48	B2 1225+317
WP700510.....	10.7	171.18	38.76	1122+39
WP700516.....	25.2	330.77	−18.92	MT FIELD
WP700535.....	9.6	217.13	42.67	4U 1417+42
WP700557.....	28.7	180.80	44.55	NGC 4051
WP700774.....	8.9	151.08	5.22	1001+054
WP701034.....	9.6	203.10	11.11	MKN 789
WP701045A01.....	12.7	354.09	2.16	ARP 284
WP701046N00.....	9.2	334.87	29.39	ARP 278
WP701048.....	13.9	21.14	3.80	520
WP701056.....	11.0	185.34	30.18	2A 1218+304
WP701059N00.....	9.5	178.30	80.97	S5 1150+81
WP701062.....	9.5	204.07	27.08	CFHT FIELD A/1
WP701063.....	10.0	205.71	27.08	CFHT FIELD A/2
WP701064.....	8.4	204.40	26.63	CFHT FIELD A/3
WP701065.....	9.0	204.40	27.53	CFHT FIELD A/4
WP701066.....	9.1	204.89	26.35	CHFT FIELD A/5
WP701067.....	8.2	204.88	27.82	CHFT FIELD A/6
WP701069.....	9.9	205.37	27.53	CHFT FIELD A/8
WP701080N00.....	16.1	259.91	48.07	1718+481

TABLE 1—*Continued*

Sequence	Exposure Time (ks)	α (deg)	δ (deg)	Target Name
WP701092	9.1	2.62	10.97	III ZW 2
WP701095N00	8.1	185.59	4.22	PKS 1219+044
WP701122N00	9.4	163.01	61.42	ABLS QSO J1052+6
WP701200	10.6	261.55	74.52	RX J1726.2+7431
WP701201N00	11.7	174.80	33.02	MS 1136.5+3413
WP701202	13.6	180.31	−3.68	MS 1158.6−0323
WP701252N00	8.6	323.12	10.14	II ZW 136
WP701457N00	27.4	255.25	64.20	HS 1700+6416
WP701458N00	18.6	146.43	−14.33	NGC 2992
WP701499N00	18.7	24.92	17.89	PKS 0136+176
WP701500N00	17.8	208.53	−2.10	PKS 1351−018
WP701501N00	12.8	358.62	−15.22	PKS 2351−154
WP701523N00	24.8	267.16	68.70	MRK 507
WP701524N00	13.1	190.43	35.06	12393+3520
WP701526N00	10.4	239.26	63.84	15564+6359
WP701552N00	13.6	248.27	41.96	RX J16331+4157
WP701554N00	12.2	147.42	29.92	PG 0946+301
WP701587N00	11.0	146.94	7.42	3C 227
WP701588N00	9.8	203.22	2.01	3C 287.1
WP701589N00	10.1	244.43	32.37	3C 332
WP701630N00	18.3	343.52	−17.58	MR 2251−179
WP900029	122.1	163.02	57.37	THE LOCKMAN FIEL
WP900207	18.7	252.65	61.08	DRACO NEB.HVC IN
WP900208	8.4	254.02	57.28	HVC/IVC 86.0,38.0
WP900212	19.5	192.81	25.66	NGC 4725/NGC 4747
WP900381N00	11.0	243.97	59.70	HVC 1
WP900382N00	9.3	168.94	42.54	M1-X1
WP900383N00	11.9	170.31	43.29	M1-X2
WP900384N00	10.4	172.18	43.01	M1-X3
WP900400A01	13.3	154.82	52.75	LOCKMAN SPUR A
WP900401A01	16.1	156.81	53.49	LOCKMAN SPUR B
WP900528N00	10.7	155.17	39.25	HVC 1
WP900529N00	10.3	157.07	38.98	HVC 2
WP900582N00	8.9	250.70	70.79	IVC- A1
WP900583N00	8.2	246.84	72.03	IVC- A2
WP900586N00	11.2	253.02	68.21	IVC- A3
WP900590N00	20.0	252.24	53.60	LVC 1
WP900591N00	15.4	254.18	52.94	LVC 2

one $z > 1$ cluster (WARP J1415.1+3612, a $z = 1.013$ cluster in WARPS I), and effectively limits our selection to $z \lesssim 1.1$.

About two-thirds of the imaging for WARPS-II was done from Hawaii (58% from the University of Hawaii 2.2 m telescope, 7% from Keck-II, and 2% from the CFHT 3.6 m telescope), whereas the remainder was done at the KPNO 2.1 m and WIYN telescopes. In contrast, WARPS-I imaging was carried out in a more heterogeneous manner from telescopes in both hemispheres. We identified 125 clusters, of which 107 are above our flux limit in total flux of 6.5×10^{-14} ergs cm^{-2} s^{-1} in the 0.5–2.0 keV band. On the basis of the spectroscopic follow-up, we found five extended X-ray sources to consist of contributions from more than one bona fide cluster, each of which is at a different redshift. We separated these sources in our catalog and estimated the flux due to each component via manual aperture photometry measurements of the *ROSAT* images.

3. CLUSTERS OF GALAXIES

3.1. *The Cluster Catalog*

In Table 2 we have listed all members of the statistically complete, flux-limited WARPS-II cluster sample. Similarly, in Table 3 we list clusters detected below the flux limit (6.5×10^{-14} ergs cm^{-2} s^{-1}). The columns in Table 2 and Table 3 are as follows:

1. The assigned cluster name. Many WARPS-II clusters have been previously identified, mostly by other serendipitous cluster surveys similar to WARPS (see § 4). In Table 4 we list the known aliases for clusters in the WARPS-II sample. The alternate names are usually listed as they appear in NASA/IPAC Extragalactic Database (NED).
2. The right ascension (in decimal degrees) in J2000.0 coordinates.
3. The declination (in decimal degrees) in J2000.0 coordinates.
4. The hydrogen column density from Dickey & Lockman (1990) in units of 10^{20} cm^{-2}.
5. The unabsorbed source flux in units of 10^{-14} ergs cm^{-2} s^{-1} in the 0.5–2.0 keV band. We calculated the final flux from the total count rate using the same iterative method as Ebeling et al. (1998). We assume a Raymond-Smith spectrum with the measured cluster redshift (see § 2.3), a metal abundance of 0.3 solar, and the hydrogen column density for the cluster coordinates from Dickey & Lockman (1990). The temperature of the model was derived

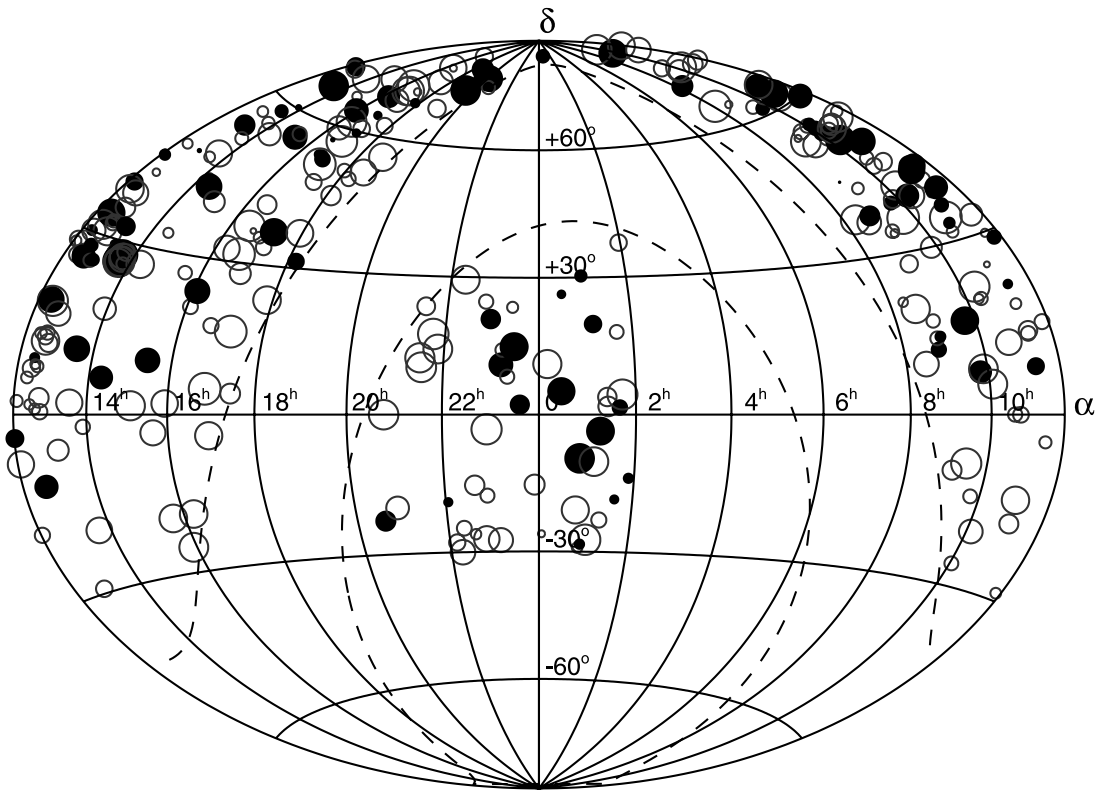

FIG. 1.—Aitoff projected distribution of WARPS-II *ROSAT* fields in equatorial coordinates. The dashed lines indicate the $|b| < 20^\circ$ range excluded. Also excluded were $\delta < -30^\circ$ and $2^h < \alpha < 8^h$. We detected clusters in the fields marked with filled circles but not in those marked with open circles. The circle size is weighted by the exposure time, which ranges from approximately 8 to 70 ks.

iteratively by constraining the cluster to obey the *L-T* relation, $T_X = 2.76 L_{bol}^{0.33}$ keV (White et al. 1997).

6. The log of the rest-frame source luminosity in units of ergs s^{-1} in the 0.5–2.0 keV band derived in the same manner as the flux. We assumed $q_0 = 0.5$ and $H_0 = 50$ km s^{-1} Mpc^{-1}, but also list in parentheses the luminosities calculated using a $H_0 = 70$, $\Omega_M = 0.3$, $\Omega_\Lambda = 0.7$ cosmology.

7. The redshift of the cluster with the number of galaxy redshifts used to derive the cluster redshift indicated in parentheses.

8. The estimated core radius of the clusters in arcseconds, assuming a King profile with $\beta = 2/3$. Note that these should be interpreted with caution given the size of the *ROSAT* PSF. Clusters that we split on the basis of redshift or other information do not have measured core radii.

9. Notes or comments (if any) about the source. See § 3.2 for more details about many of these sources.

In Figure 2 we provide a finder chart for each cluster with the X-ray emission contours overlaid on optical images of the cluster. The source of the optical image (usually a CCD image but occasionally a Digitized Sky Survey image) is indicated in the upper left corner, along with the exposure time and band. These finder charts, as well as other information, are also available on our Web site. Figure 3 shows a histogram of the redshift distribution of the sample. The clusters in WARPS-II range in redshift from $z = 0.03-0.92$ with a median redshift of $z = 0.29$. We have 59 clusters at $z > 0.3$ and 11 at $z > 0.6$. Figure 4 shows the distribution of the clusters in the L_X-z plane. For comparison we also plot the clusters in two *ROSAT* All-Sky Survey based samples, the Brightest Cluster Survey (Ebeling et al. 1998) and Northern *ROSAT* All-Sky Survey (Böhringer et al. 2000). WARPS covers the region of phase space at lower luminosities and higher redshifts.

3.2. *Comments on Individual Clusters*

In this section, we provide additional information and details about many of the clusters in the WARPS-II sample.

WARP J0030.5+2618.—Spectroscopic follow-up of this source found three galaxies with an average redshift of $z = 0.4995$ and two galaxies with an average redshift of $z = 0.2677$. We also have poor SNR spectra for four other galaxies with $z \approx 0.50$ for two and $z \approx 0.27$ for the other two. We have assigned all the cluster flux to the higher redshift cluster based on the X-ray morphology and the coincidence of the X-ray centroid with a $z = 0.5$ galaxy with the appearance of a brightest cluster galaxy (BCG). However, there may be contamination from a lower redshift structure along the line of sight. The *Chandra* observation (Maughan et al. 2008) shows a flux of $2.29 \pm 0.27 \times 10^{-13}$ ergs cm^{-2} s^{-1}, consistent with our measurement to within the errors.

WARP J0035.9+8513.—This distant cluster ($z = 0.83$) has very low X-ray surface brightness but is clearly extended. There are three galaxies close to each other and near the X-ray centroid that all have concordant redshifts (although one spectrum has low SNR). The cluster's existence has been confirmed by an *XMM-Newton* observation, and the 0.5–2.0 keV flux within the virial radius is estimated to be 4.6×10^{-14} ergs cm^{-2} s^{-1}, below our flux limit. However, the *XMM-Newton* observation was badly affected by flares, and the remaining portion of the observation contained only about 200 counts for the cluster, so the SNR is low. Given the uncertainty in extrapolating the *XMM-Newton* surface brightness profile (since the best fit has an unusually flat β-value of $0.52^{+0.15}_{-0.09}$) and the unknown temperature, the uncertainty in the *XMM-Newton* flux value is large and does not rule out the true flux being above the survey flux limit. Thus, we use the *ROSAT* flux and include the cluster in the statistically complete sample.

TABLE 2

WARPS-II Statistically Complete, Flux-limited Sample

Name (1)	α (deg) (2)	δ (deg) (3)	$n_{\rm H}$ (10^{20} cm^{-2}) (4)	Flux (10^{-14} cgs) (5)	log $L_{\rm x}$ (ergs s^{-1}) (6)	z (7)	r_c (arcsec) (8)	Comments (9)
WARP J0026.7+0501	6.6992	5.0238	3.32	11.73	43.63 (43.33)	0.2529 (8)	22.9	
WARP J0030.5+2618	7.6390	26.3069	3.86	21.43	44.53 (44.24)	0.5000 (2)	22.8	Contaminated? See § 3.2.
WARP J0035.9+8513	8.9969	85.2215	7.91	8.40	44.62 (44.33)	0.8317 (2)	35.9	
WARP J0046.3+8530	11.5809	85.5158	7.22	16.79	44.64 (44.35)	0.6241 (1)	22.5	
WARP J0050.9−0928	12.7479	−9.4830	3.79	31.54	43.83 (43.54)	0.2010 (2)	25.0	
WARP J0054.0−2824	13.5152	−28.4062	1.80	7.81	43.60 (43.30)	0.2927 (8)	17.8	
WARP J0057.4+3012	14.3735	30.2143	5.92	10.11	42.89 (42.59)	0.1230 (3)	32.7	
WARP J0110.3+1938	17.5836	19.6480	3.74	9.80	43.76 (43.47)	0.3152 (2)	30.2	
WARP J0116.6−0329	19.1673	−3.4991	4.08	28.20	42.94 (42.63)	0.0800 (2)	38.6	
WARP J0136.4−1811	24.1024	−18.1971	1.42	6.81	43.38 (43.09)	0.2490 (2)	28.9	
WARP J0139.6+0119	24.9106	1.3241	3.03	13.65	43.69 (43.39)	0.2520 (3)	33.8	
WARP J0152.7−1357	28.1755	−13.9652	1.47	30.02	45.15 (44.85)	0.8325 (5)	27.5	
WARP J0819.3+7054	124.8368	70.9148	3.40	13.95	43.60 (43.30)	0.2260 (?)	28.7	
WARP J0849.1+3731	132.2897	37.5308	2.90	26.63	43.93 (43.63)	0.2400 (?)	38.8	
WARP J0851.9+1159	132.9910	11.9954	3.77	14.67	42.99 (42.69)	0.1150 (?)	35.4	
WARP J0858.4+1357	134.6054	13.9545	3.84	6.96	44.03 (43.74)	0.4850 (?)	13.3	
WARP J0937.1+6116	144.2759	61.2828	2.82	8.14	43.27 (42.97)	0.2040 (2)	37.2	
WARP J0942.3+8111	145.5883	81.1858	1.93	21.23	44.61 (44.31)	0.5450 (2)	14.1	
WARP J0943.5+1639	145.8842	16.6644	3.43	21.80	43.90 (43.61)	0.2560 (?)	33.4	
WARP J0943.7+1644	145.9320	16.7386	2.82	13.81	43.38 (43.08)	0.1800 (?)	34.3	
WARP J0947.9+0730	146.9825	7.5110	3.05	8.54	42.86 (42.55)	0.1280 (?)	40.5	
WARP J1002.6−0808	150.6714	−8.1460	4.73	11.52	44.32 (44.03)	0.5240 (2)	28.5	
WARP J1010.1+5430	152.5469	54.5010	0.73	30.38	42.45 (42.13)	0.0450 (2)	32.7	
WARP J1011.0+5339	152.7573	53.6626	0.73	8.49	43.72 (43.43)	0.3200 (4)	25.1	
WARP J1011.0+5358	152.7509	53.9682	0.73	8.63	43.87 (43.58)	0.3720 (?)	27.7	
WARP J1011.5+5450	152.8926	54.8344	0.73	6.90	43.55 (43.25)	0.2940 (?)	14.5	
WARP J1020.2+3913	155.0665	39.2295	1.39	9.91	43.04 (42.74)	0.1463 (2)	28.6	
WARP J1020.5+3922	155.1269	39.3797	1.43	7.38	42.90 (42.59)	0.1430 (2)	24.3	
WARP J1023.1+4124	155.7752	41.4131	1.12	8.40	43.41 (43.11)	0.2320 (2)	42.1	
WARP J1038.0+4147	159.5063	41.7845	1.34	26.00	43.31 (43.01)	0.1250 (2)	36.3	
WARP J1049.7+3308	162.4367	33.1438	2.00	8.95	43.43 (43.13)	0.2300 (2)	13.4	
WARP J1056.2+4933	164.0516	49.5565	1.19	14.39	43.49 (43.19)	0.1990 (?)	50.7	
WARP J1058.8+6223	164.7098	62.3984	0.97	8.89	43.87 (43.58)	0.3700 (2)	41.9	
WARP J1059.9+6421	164.9973	64.3523	1.17	9.53	43.28 (42.98)	0.1920 (2)	22.8	
WARP J1103.6+3555	165.9047	35.9216	1.82	7.03	44.48 (44.19)	0.7750 (3)	15.3	
WARP J1104.4+3600	166.1248	36.0057	2.06	6.59	44.03 (43.74)	0.4970 (2)	4.5	
WARP J1117.4+0743	169.3599	7.7254	5.17	9.16	44.15 (43.86)	0.4859 (4)	22.1	
WARP J1117.5+0746	169.3753	7.7772	3.36	8.76	43.04 (42.74)	0.1550 (1.5)	31.1	
WARP J1119.4+2106	169.8638	21.1154	1.22	10.32	43.23 (42.93)	0.1740 (3)	6.6	
WARP J1120.1+4318	170.0302	43.3032	2.26	35.04	44.93 (44.63)	0.6120 (3)	11.1	
WARP J1124.7+3859	171.1957	38.9954	2.07	7.61	43.61 (43.32)	0.3014 (3)	24.8	
WARP J1127.7+4310	171.9439	43.1740	2.13	17.85	44.11 (43.81)	0.3470 (2)	30.3	
WARP J1128.9+4251	172.2258	42.8631	2.23	18.10	44.28 (43.99)	0.4140 (2)	45.4	
WARP J1134.2+5952	173.5592	59.8764	1.06	8.45	43.62 (43.33)	0.2900 (?)	33.1	
WARP J1142.1+1009	175.5299	10.1538	3.11	31.36	43.34 (43.04)	0.1178 (?)	50.2	
WARP J1142.2+1026	175.5692	10.4487	3.00	24.34	43.45 (43.15)	0.1500 (1)	26.0	
WARP J1146.4+2854	176.6223	28.9014	1.70	37.04	43.62 (43.33)	0.1488 (3)	49.9	
WARP J1200.8−0327	180.2059	−3.4616	2.43	19.41	44.27 (43.98)	0.3967 (2)	32.0	
WARP J1204.3−0351	181.0973	−3.8533	2.66	8.83	43.54 (43.24)	0.2610 (?)	26.4	
WARP J1205.8+4429	181.4658	44.4872	1.32	7.96	44.28 (43.99)	0.5921 (1)	12.7	
WARP J1211.2+3911	182.8163	39.1952	1.95	33.86	44.36 (44.06)	0.3400 (?)	21.2	
WARP J1217.2+6940	184.3107	69.6697	1.76	8.62	42.69 (42.38)	0.1070 (2)	26.4	
WARP J1218.4+3011	184.6211	30.1962	1.69	8.82	43.85 (43.55)	0.3600 (1)	24.2	
WARP J1220.9+1810	185.2320	18.1755	2.57	11.60	44.13 (43.84)	0.4294 (3)	25.7	
WARP J1226.9+3332	186.7400	33.5493	1.38	35.06	45.28 (44.99)	0.8945 (2)	8.4	
WARP J1227.2+0858	186.8075	8.9696	1.73	48.84	43.28 (42.98)	0.0900 (?)	56.1	
WARP J1235.9+2742	188.9877	27.7117	0.00	9.08	43.92 (43.62)	0.3821 (2)	26.5	Contaminated? See § 3.2.
WARP J1236.9+2550	189.2299	25.8492	1.34	23.04	43.56 (43.26)	0.1720 (3)	58.0	
WARP J1240.4−1147	190.1041	−11.7931	3.84	13.70	43.44 (43.15)	0.1930 (2)	30.8	
WARP J1254.6+2545	193.6624	25.7557	0.81	11.26	43.36 (43.06)	0.1930 (?)	27.7	
WARP J1254.8+2550	193.7221	25.8469	0.88	11.09	43.53 (43.23)	0.2330 (2?)	27.5	
WARP J1256.0+2556	194.0143	25.9467	0.90	10.62	43.51 (43.21)	0.2322 (3)	21.4	
WARP J1308.5+5342	197.1352	53.7001	1.65	23.16	44.16 (43.87)	0.3260 (?)	32.9	
WARP J1311.2+3229	197.8041	32.4868	1.10	52.12	44.23 (43.94)	0.2450 (?)	26.0	

TABLE 2—*Continued*

Name (1)	α (deg) (2)	δ (deg) (3)	$n_{\rm H}$ (10^{20} cm^{-2}) (4)	Flux (10^{-14} cgs) (5)	log $L_{\rm x}$ (ergs s^{-1}) (6)	z (7)	r_c (arcsec) (8)	Comments (9)
WARP J1316.0+2856S	199.0167	28.9222	1.10	8.61	43.50 (43.20)	0.2530 (?)	...	See § 3.2
WARP J1325.2+6550	201.3121	65.8392	2.01	14.52	43.40 (43.11)	0.1800 (?)	51.6	
WARP J1329.9+5834	202.4926	58.5692	1.39	8.73	43.67 (43.38)	0.3020 (2)	34.0	
WARP J1330.9+5814	202.7462	58.2488	1.39	15.06	43.93 (43.63)	0.3100 (3)	29.2	
WARP J1331.5+1108	202.8758	11.1344	1.94	9.82	42.54 (42.22)	0.0850 (2)	6.9	
WARP J1337.1+2649	204.2955	26.8256	1.04	9.53	44.00 (43.71)	0.4100 (?)	32.5	
WARP J1337.8+2639	204.4579	26.6543	1.04	15.00	44.01 (43.72)	0.3400 (?)	17.2	
WARP J1342.8+4028	205.7032	40.4719	0.84	8.94	44.48 (44.19)	0.6990 (3)	18.3	
WARP J1350.8+6007	207.7097	60.1256	1.64	12.79	44.75 (44.46)	0.7960 (2)	30.1	
WARP J1419.3+0638	214.8437	6.6387	2.16	14.35	44.45 (44.16)	0.5487 (4)	13.4	
WARP J1419.9+0634E	214.9929	6.5722	2.16	9.45	44.32 (44.03)	0.5740 (?)	...	
WARP J1419.9+0634W	214.9692	6.5722	2.16	7.48	44.21 (43.92)	0.5641 (?)	...	
WARP J1429.0+4241	217.2743	42.6867	1.34	6.91	44.64 (44.35)	0.9200 (?)	3.1	
WARP J1514.9+5541	228.7299	55.6912	1.47	10.50	44.34 (44.05)	0.5590 (2)	13.5	
WARP J1524.0+1003	231.0173	10.0540	2.88	12.63	43.53 (43.24)	0.2200 (3)	35.5	
WARP J1524.6+0957	231.1652	9.9601	2.88	33.79	44.75 (44.46)	0.5170 (3)	24.2	
WARP J1524.8+1005	231.2176	10.0882	2.88	6.87	43.40 (43.10)	0.2510 (?)	0.1	
WARP J1606.7+2329	241.6825	23.4862	4.84	14.91	43.92 (43.63)	0.3100 (?)	38.6	
WARP J1614.4+6825	243.6036	68.4281	3.85	7.04	42.78 (42.47)	0.1280 (?)	28.9	
WARP J1639.8+5347	249.9584	53.7964	2.55	130.70	43.86 (43.56)	0.1070 (?)	96.9	
WARP J1649.2+5325	252.3008	53.4174	2.75	162.80	42.79 (42.47)	0.0290 (?)	112.2	
WARP J1657.8+5301	254.4517	53.0291	2.73	14.74	44.33 (44.04)	0.4790 (2)	8.3	
WARP J1658.0+5254	254.5208	52.9015	2.73	14.25	44.29 (44.00)	0.4655 (?)	19.0	
WARP J1702.2+6419	255.5591	64.3320	2.46	8.77	43.39 (43.10)	0.2240 (?)	39.0	
WARP J1746.3+6849E	266.6375	68.8139	4.23	6.72	43.58 (43.29)	0.3070 (?)	...	
WARP J1746.3+6849W	266.5792	68.8306	4.23	15.05	43.53 (43.23)	0.2030 (?)	...	
WARP J1812.0+3113	273.0065	31.2202	4.89	9.06	43.41 (43.11)	0.2246 (10)	15.5	
WARP J1843.5+7950	280.8796	79.8354	4.11	16.09	42.29 (41.99)	0.0510 (3)	15.9	
WARP J1930.5+7403W	292.5479	74.0597	8.23	11.19	43.74 (43.45)	0.2910 (?)	...	
WARP J2002.6+7753	300.6602	77.8960	8.57	39.08	44.44 (44.15)	0.3492 (3)	21.2	
WARP J2009.9+7744	302.4758	77.7418	9.59	12.31	43.95 (43.66)	0.3461 (2)	25.8	
WARP J2036.6−2247	309.1661	−22.7891	4.02	26.36	43.65 (43.36)	0.1800 (2)	64.3	
WARP J2202.7−1902	330.6831	−19.0385	2.66	10.68	44.11 (43.82)	0.4359 (3)	42.3	
WARP J2257.8+2056	344.4604	20.9423	5.24	9.62	43.69 (43.40)	0.2961 (9)	15.3	
WARP J2258.1+2055	344.5353	20.9180	5.24	53.22	44.39 (44.10)	0.2880 (?)	22.1	
WARP J2312.7+1043	348.1781	10.7250	4.30	16.06	43.95 (43.66)	0.3100 (2)	24.9	
WARP J2328.8+1453	352.2074	14.8860	4.05	7.33	44.07 (43.79)	0.4954 (3)	24.0	
WARP J2335.6+0217	353.9048	2.2915	4.68	6.55	43.79 (43.50)	0.3877 (3)	17.1	

WARP J0046.3+8530.—Although we only have two galaxy redshifts, the cluster redshift is confirmed by an *XMM-Newton* X-ray redshift measurement of $z = 0.615^{+0.008}_{-0.006}$ (Maughan et al. 2004b), consistent with the BCG redshift of $z = 0.6243 \pm 0.0004$. The *XMM-Newton* flux of $1.45 \pm 0.07 \times 10^{-13}$ ergs cm^{-2} s^{-1} (0.5–2.0 keV) extrapolated to the virial radius is in reasonable agreement with the *ROSAT* flux. The slightly higher value of the *ROSAT* flux is due to the inclusion of unresolved (or barely resolved) point sources.

WARP J0152.7−1357.—The discovery of this massive and luminous cluster was first reported in Paper III. It is a high-redshift ($z = 0.83$) system composed of two subclusters likely in the process of merging. Follow-up observations have been done by *BeppoSAX* (Della Ceca et al. 2000), *Chandra* (Maughan et al. 2003), and *XMM-Newton* (Maughan et al. 2006a). A number of other groups have published observations of this cluster with *HST* (Huo et al. 2004; Jee et al. 2005; Postman et al. 2005; Holden et al. 2005), the VLT (Demarco 2005), and Gemini (Jorgensen et al. 2005) observatories. Subsequent analysis of *Einstein* data has revealed that it was missed in the original *Einstein* Extended Medium Sensitivity Survey sample (Lewis et al. 2002). Along with WARP J1226.9+3332 and MS 1054.4−0321, this cluster was one the first three imaged using the Sunyaev-Zeldovich effect (Joy et al. 2001). The *Chandra* flux of $1.83^{+0.22}_{-0.18} \times 10^{-13}$ ergs cm^{-2} s^{-1} (0.5–2.0 keV; Maughan et al. 2003) is slightly lower than the *ROSAT* value, due to unresolved (or barely resolved) point-source contamination of the *ROSAT* flux.

WARP J0848.8+4456.—This system was explored in detail by Holden et al. (2001) as part of a *Chandra* follow-up of the RDCS. They find that it consists of an X-ray–emitting cluster of galaxies at a redshift of $z = 0.570$ (similar to our redshift value) and a group at a slightly lower redshift, $z = 0.543$, with little X-ray emission. The lower redshift system contains a gravitationally lensed arc. The *Chandra* observation (Maughan et al. 2008) shows a flux of $3.77 \pm 0.05 \times 10^{-14}$ ergs cm^{-2} s^{-1}, consistent with our measurement to within the errors.

WARP J1008.7+5342.—The *ROSAT* flux of this distant cluster ($z = 0.872$) of $5.2 \pm 0.8 \times 10^{-14}$ ergs cm^{-2} s^{-1} (0.5–2.0 keV), extrapolated to the virial radius, is well below the cluster's *ROSAT* flux of 7.31×10^{-14} ergs cm^{-2} s^{-1}. The *XMM-Newton* image shows two point sources, respectively, northeast and west of the cluster (Maughan et al. 2006b) and each about an arcminute away, with approximate fluxes of 0.8×10^{-14} and 0.5×10^{-14} ergs cm^{-2} s^{-1}, respectively. The *ROSAT* image

TABLE 3
WARPS-II Additional Clusters and Candidates

Name (1)	α (deg) (2)	δ (deg) (3)	$n_{\rm H}$ (10^{20} cm^{-2}) (4)	Flux (10^{-14} cgs) (5)	log $L_{\rm x}$ (ergs s^{-1}) (6)	z (7)	r_c (arcsec) (8)	Comments (9)
WARP J0848.8+4456	132.2000	44.9405	2.81	4.09	43.98 (43.69)	0.5740 (?)	13.1	
WARP J0941.0+3843	145.2518	38.7187	1.59	6.27	43.49 (43.19)	0.2870 (4)	40.1	
WARP J1008.7+5342	152.1992	53.7009	0.76	7.31	44.61 (44.32)	0.8720 (2)	20.3	Contaminated. See § 3.2
WARP J1010.9+5557	152.7426	55.9626	0.89	5.51	42.94 (42.64)	0.1710 (1)	17.8	
WARP J1011.3+5333	152.8460	53.5631	0.79	5.88	43.76 (43.46)	0.3900 (3)	27.2	
WARP J1019.6+3920	154.9052	39.3423	1.43	6.08	43.73 (43.43)	0.3730 (2)	20.4	
WARP J1020.9+5132	155.2467	51.5485	0.93	5.60	43.98 (43.69)	0.5019 (3)	9.3	
WARP J1119.7+2126	169.9321	21.4471	1.49	4.80	41.93 (41.65)	0.0610 (?)	6.3	See § 3.2
WARP J1125.3+3854	171.3460	38.9017	2.06	5.71	44.07 (43.78)	0.5477 (?)	14.9	
WARP J1142.6+1028	175.6640	10.4733	3.00	6.18	43.08 (42.78)	0.1880 (2)	0.0	
WARP J1205.0−0332	181.2618	−3.5490	2.66	4.42	43.58 (43.29)	0.3680 (?)	22.7	
WARP J1205.5+4419	181.3873	44.3191	1.24	6.35	43.65 (43.36)	0.3384 (2)	22.2	
WARP J1206.1+4419	181.5278	44.3245	1.24	6.12	43.50 (43.21)	0.2946 (3)	25.2	
WARP J1247.7−0548	191.9299	−5.8158	2.12	6.07	43.49 (43.20)	0.2928 (2)	8.7	
WARP J1256.6+4715	194.1631	47.2583	1.19	6.18	43.81 (43.52)	0.4040 (3)	19.0	
WARP J1338.4+2644	204.6028	26.7444	1.04	6.24	41.38 (41.10)	0.0290 (2)	12.4	
WARP J1339.0+2745	204.7676	27.7566	1.07	13.20	43.06 (42.76)	0.1300 (?)	9.8	Sy2, See § 3.2
WARP J1514.2+5527	228.5561	55.4642	1.47	5.70	43.93 (43.64)	0.4753 (3)	27.2	
WARP J1559.1+6353	239.7916	63.8849	1.87	8.42	44.64 (44.35)	0.8500 (?)	21.6	Contaminated. See § 3.2.
WARP J1633.6+5714	248.4206	57.2375	1.84	5.41	43.25 (42.95)	0.2390 (?)	23.6	
WARP J1703.1+5938	255.7890	59.6478	1.97	5.86	43.03 (42.73)	0.1822 (3)	25.5	
WARP J1715.8+3656	258.9688	36.9372	3.37	4.97	42.31 (42.01)	0.0910 (3)	6.0	
WARP J1941.2+7709E	295.4292	77.1625	6.44	5.26	41.75 (41.48)	0.0480 (?)	...	

shows visible elongation in the direction of these two point sources. It seems likely that the *ROSAT* flux is thus point-source contaminated, so we do not include this cluster in the statistically complete sample. Although we based our redshift for this cluster on only two spectra, it is supported by several spectra with poorer SNR.

WARP J1011.3+5333.—The northern part of this source is a cluster at $z = 0.39$. The southern part is probably point-source contamination, or an unrelated source, since the galaxy near the peak of the southern part has $z = 0.229$. We estimate that the 65% of the total flux is due to the northern part and have reduced the flux accordingly. This reduction puts the cluster below our flux limit for inclusion in our statistical sample.

WARP J1103.6+3555.—The *ROSAT* flux is in good agreement (within the errors) with the *XMM-Newton* flux of $(6.3 \pm 0.4) \times 10^{-14}$ ergs cm^{-2} s^{-1} (0.5–2.0 keV) extrapolated to the virial radius (Maughan et al. 2006b). No point-source contamination is visible in either the PSPC or *XMM-Newton* images.

WARP J1117.4+0743.—We find $z = 0.4859$ ($n_z = 4$) but also $z = 0.301$ ($n_z = 2$, both with blue continua). All six galaxies are in a fairly compact region close to (but not coincident with) the PSPC centroid. A weak HRI signal confirms the detection without sufficient SNR to confirm the extended nature. On the basis of the galaxy magnitudes and the higher number of redshifts, we assign all the X-ray flux to the higher redshift cluster.

WARP J1119.7+2126.—This source was identified as a possible fossil group by Jones et al. (2003). A giant elliptical galaxy at the peak of the X-ray emission completely dominates the group. There is an excess of faint galaxies visible within the X-ray contours. Two nearby galaxies are spectroscopically confirmed group members but are 3.3–3.4 mag fainter.

WARP J1120.1+4318.—We find some spectroscopic evidence for structure at two redshifts, with $z = 0.612$ ($n_z = 3$) and $z = 0.30$ ($n_z = 2$). However, based on the X-ray morphology, and especially the X-ray redshift of $z = 0.61 \pm 0.03$ from an *XMM-Newton* spectrum (Arnaud et al. 2002), we assign all the cluster flux to the higher redshift system.

WARP J1142.2+1026.—Our redshift for this cluster is based on one good-quality and another lower quality spectrum at $z = 0.15$. Therefore, our redshift for this cluster is not secure.

WARP J1226.9+3332.—We first reported the discovery of this cluster in Paper V, and it has subsequently been the subject of many follow-up observations. It is among the most distant ($z = 0.89$) and X-ray luminous galaxy clusters known. Sunyaev-Zeldovich imaging confirmed that it is a massive cluster (Joy et al. 2001). Cagnoni et al. (2001) present optical and near-IR imaging of the cluster as well as the results of *Chandra* observations, and Ellis & Jones (2004) give the *K*-band galaxy luminosity function. The *ROSAT* flux is in good agreement with the *XMM-Newton* flux of $(3.7 \pm 0.1) \times 10^{-13}$ ergs cm^{-2} s^{-1} (0.5–2 keV) and the *Chandra* flux of $(3.6 \pm 0.1) \times 10^{-13}$ ergs cm^{-2} s^{-1} (0.5–2 keV), both extrapolated to the virial radius (Maughan et al. 2004a, 2007). Thus, there is no significant point-source contamination of the *ROSAT* flux.

WARP J1235.9+2742.—The peak of the PSPC emission is coincident with the peak of extended HRI emission, but the PSPC centroid is offset slightly, in the direction of a possible contaminating source (or extended low surface brightness emission). However, no possible contaminating source is visible in a deep HRI image. We note that the PSPC flux (by ~20%) and position (by $\approx 15''$) may be incorrect for this reason.

WARP J1256.0+2556.—This source was identified as a possible fossil group by Jones et al. (2003). Optically this source is a rich group of galaxies, dominated by a luminous elliptical galaxy, with fainter galaxies observed in projection against it. The classification as a fossil system is somewhat uncertain since it depends on whether a group galaxy located at about half the virial radius is included.

TABLE 4

ALTERNATE NAMES FOR WARPS-II CLUSTERS

WARPS Name	Other Names
WARP J0026.7+0501	GHO 0024+0444
WARP J0030.5+2618	VMF98 001, RX J0030.5+2618 (BSHARC2), CRSS J0030.5+2618
WARP J0050.9−0928	VMF98 003
WARP J0054.0−2824	VMF98 004
WARP J0110.3+1938	VMF98 008
WARP J0136.4−1811	VMF98 015
WARP J0139.6+0119	VMF98 016, ZWCL 0137.0+0107
WARP J0152.7−1357	RX J0152.7−1357 (BSHARC)
WARP J0819.3+7054	VMF98 049
WARP J0848.8+4456	VMF98 060, RX J0848.7+4457 (BSHARC2)
WARP J0849.1+3731	VMF98 062, ABELL 0708, RX J0849.1+3731 (BSHARC), RX J084907.0+373158 (RIXOS)
WARP J0858.4+1357	VMF98 066, RX J085825.9+135724 (RIXOS), RX J0858.4+1357 (SSHARC)
WARP J0937.1+6116	ZWCL 0933.6+6127
WARP J0943.5+1639	VMF98 073, RX J094330.7+164002 (RIXOS)
WARP J0943.7+1644	VMF98 074, ZWCL 0941.4+1658, RX J094344.9+164448 (RIXOS)
WARP J0947.9+0730	RX J0947.9+0730 (SSHARC)
WARP J1002.6−0808	VMF98 083, 1WGA J1002.6−0808
WARP J1010.1+5430	VMF98 084, RX J101014.2+542958 (RIXOS), RXC J1010.2+5429
WARP J1010.9+5557	ABELL 0935
WARP J1011.0+5339	VMF98 085
WARP J1011.5+5450	VMF98 086, RX J101134.9+544956 (RIXOS)
WARP J1020.2+3913	RX J1020.0+3915 (BSHARC2)
WARP J1020.5+3922	RX J1020.2+3926 (BSHARC2)
WARP J1056.2+4933	VMF98 094, RX J105612.7+493306 (RIXOS)
WARP J1059.9+6421	ZWCL 1056.5+6437
WARP J1117.4+0743	VMF98 097
WARP J1117.5+0746	RX J111730.1+074618 (RIXOS)
WARP J1119.4+2106	RX J111927.0+210651 (RIXOS), RX J1119.4+2106 (BSHARC2)
WARP J1119.7+2126	VMF98 099, RX J111943.7+212643 (RIXOS)
WARP J1120.1+4318	RX J1120.1+4318 (BSHARC)
WARP J1127.7+4310	MS 1125.3+4324
WARP J1134.2+5952	ZWCL 1131.2+6009
WARP J1142.1+1009	ABELL 1354, RX J1142.0+1009 (SSHARC)
WARP J1142.2+1026	RX J1142.2+1026 (BSHARC), RX J1142.2+1027 (SSHARC)
WARP J1146.4+2854	VMF98 107, RX J114621.27+285320
WARP J1200.8−0327	VMF98 111, RX J120049.1−032738 (RIXOS), RX J1200.8−0327 (BSHARC2), RX J1200.8−0328 (SSHARC)
WARP J1204.3−0351	VMF98 113, RX J1204.3−0350, RX J1204.3−0351 (BSHARC2)
WARP J1205.0−0332	RX J1205.0−0333 (SSHARC)
WARP J1205.8+4429	RX J1205.8+4429 (BSHARC2)
WARP J1211.2+3911	VMF98 115, MS 1208.7+3928, RX J1211.2+3911 (BSHARC)
WARP J1218.4+3011	VMF98 118, RX J121828.6+301150 (RIXOS)
WARP J1226.9+3332	CL J1226.9+3332, 1WGA J1226.9+3332
WARP J1227.2+0858	RX J1227.2+0858 (SSHARC)
WARP J1236.9+2550	RX J1236.9+2550
WARP J1254.6+2545	VMF98 126
WARP J1254.8+2550	VMF98 127
WARP J1256.0+2556	VMF98 128
WARP J1256.6+4715	VMF98 129, RX J125639.4+471519 (RIXOS), RX J1256.6+4715, B3 1254+475
WARP J1308.5+5342	RX J1308.5+5342 (BSHARC)
WARP J1311.2+3229	VMF98 132, MS 1308.8+3244, RX J131112.2+322907 (RIXOS), RX J1311.2+3228 (BSHARC)
WARP J1316.0+2856S	GHO 1313+2911
WARP J1325.2+6550	VMF98 134
WARP J1331.5+1108	RX J133129.9+110802 (RIXOS)
WARP J1337.8+2639	VMF98 142
WARP J1342.8+4028	VMF98 148
WARP J1419.3+0638	VMF98 161
WARP J1419.9+0634E	VMF98 162
WARP J1419.9+0634W	VMF98 162
WARP J1429.0+4241	CRSS J1429.1+4241
WARP J1524.6+0957	VMF98 170, RX J1524.6+0957 (BSHARC)
WARP J1606.7+2329	VMF98 176
WARP J1633.6+5714	VMF98 181, RX J163340.4+571410 (RIXOS)
WARP J1639.8+5347	VMF98 182, ABELL 2220
WARP J1649.2+5325	ARP 330, SHK 016
WARP J1702.2+6419	VMF98 192, RX J1702.2+6420
WARP J1746.3+6849E	VMF98 195

TABLE 4—*Continued*

WARPS Name	Other Names
WARP J1746.3+6849W	VMF98 195
WARP J2202.7−1902	VMF98 205, RX J2202.7−1902 (SSHARC)
WARP J2257.8+2056	VMF98 212
WARP J2258.1+2055	VMF98 213, MS 2255.7+2039, RX J2258.1+2055 (BSHARC)
WARP J2312.7+1043	RX J231242.9+104302 (RIXOS)
WARP J2328.8+1453	VMF98 219

NOTES.—Alternate names are listed as they appear in NED. "VMF98" refers to the 160SD catalog of Vikhlinin et al. (1998). The name in parentheses following many sources indicates the catalog from which it came: BSHARC for the Bright SHARC Survey (Romer et al. 2000), SSHARC for the Southern SHARC Survey (Burke et al. 2003), the RIXOS catalog (Mason et al. 2000), or ROXS catalog (Donahue et al. 2001).

WARP J1316.0+2856S.—The X-ray emission from the region around this cluster is complicated. It was originally included in the catalog as one source, but we excluded the northern emission component based on spectroscopic evidence that it is largely due to a QSO. The southern component appears to be a cluster at $z = 0.253$ ($n_z = 3$), but there may be additional point-source contamination. We estimate that 42% of the flux is from the southern, cluster component and have reduced the flux accordingly.

WARP J1331.5+1108.—This source was identified as a possible fossil group by Jones et al. (2003). Optically it is a fossil group with three spectroscopically confirmed group members. The X-ray emission is a probable combination of fossil group and AGN, with the X-ray luminosity of each component remaining uncertain.

WARP J1339.0+2745.—The peak of the X-ray emission is coincident with a Sy2 galaxy at $z = 0.163$ (from NED), and inspection of the X-ray image shows that most flux originates in this point source. The measured extension is due to a merger with a nearby fainter point X-ray source. Thus, although this source is in the near Abell 1769, we do not assign any X-ray flux to the Abell cluster.

WARP J1342.8+4028.—For this high-redshift cluster, we have used the redshift of $z = 0.699$ taken from the 160SD survey (Mullis et al. 2003). The *ROSAT* flux (8.94×10^{-14} ergs s^{-1} (0.5–2.0 keV) disagrees at the 2 σ level with the *XMM-Newton* value (($7.3 \pm 0.7) \times 10^{-14}$ ergs s^{-1}), most likely due to the presence of two point sources seen in the *XMM-Newton* data that may have been included in the *ROSAT* flux (Maughan et al. 2006b).

WARP J1350.8+6007.—This high-redshift cluster was detected as extended in the PSPC, a low-SNR HRI detection, and also in an *XMM-Newton* observation. The VTP detection contains an eastern source that appears pointlike, although it is not detected in the HRI observation. Removing this source reduces the flux by 18%. The eastern source is absent in the *XMM-Newton* observation, confirming its noncluster nature. The *XMM-Newton* flux of 9.0×10^{-14} ergs s^{-1} (0.5–2.0 keV), extrapolated to the virial radius, is in good agreement with the *ROSAT* flux. This cluster was also detected in the RDCS at $z = 0.804$ and confirmed in *Chandra* and weak lensing observations by Holden et al. (2002). Our redshifts of $z = 0.796$ for two galaxies is in reasonable agreement with the RDCS value. The *Chandra* luminosity of $(1.4 \pm 0.2) \times 10^{44}$ ergs cm^{-2} s^{-1} (0.5–2 keV) within 1 Mpc (which corresponds approximately to our *XMM-Newton* estimate of virial radius) is lower than our measurement of 2.7×10^{44} ergs s^{-1} (using Holden et al. cosmology), probably because of different assumptions when extrapolating the surface brightness profile.

WARP J1419.9+0634E and WARP J1419.9+0634W.—This source was discovered to be two clusters at $z = 0.574$ ($n_z = 2$) and $z = 0.564$ ($n_z = 3$). We also have two more low-SNR redshifts likely at $z = 0.57$. Therefore, we split the original detection into two components. From aperture photometry, we estimate that the $z = 0.57$ cluster has 56% of the total flux and the $z = 0.56$ cluster has 44%. Given the projected distances of the respective cluster centroids (560 kpc) and the velocity difference of $\sim$2800 km s^{-1} (about twice the typical velocity dispersion of rich clusters), it is likely that these clusters form part of a larger supercluster or filamentary system at this redshift. Further studies are needed to confirm this.

WARP J1429.0+4241.—At $z = 0.92$, this cluster is the one of the most distant detected in WARPS. It is only marginally extended but clearly coincident with a distant cluster optically. No point-source contamination is obvious in the PSPC data. *XMM-Newton* data (analysis in progress) confirm this source as a cluster with an X-ray redshift of $z = 0.94^{+0.07}_{-0.03}$ and little or no point-source contamination, as the *XMM-Newton* flux ($8.8 \pm 0.9 \times 10^{-14}$ ergs s^{-1}) is well within the errors of the *ROSAT* measurement.

WARP J1559.1+6353.—The PSPC centroid is offset by $\approx 30''$ from the HRI centroid (which is coincident with the brightest cluster galaxies), suggesting that the PSPC flux and position may be contaminated. However, no clearly resolved point source is visible in the PSPC image, and no point source that could be responsible for the contamination is visible in the HRI image. An *XMM-Newton* observation confirms that there is a relatively bright point source $1'$ south of the cluster, which was incorrectly included in the PSPC flux. The *XMM-Newton* flux from the cluster is $(0.41^{+0.05}_{-0.07}) \times 10^{-13}$ (0.5–2.0 keV) ergs cm^{-2} s^{-1} extrapolated to the virial radius, which is only $\approx$50% of the PSPC flux (Maughan et al. 2006b). Thus, this cluster falls below the survey flux limit.

WARP J1746.3+6849E and WARP J1746.3+6849W.—These two clusters were originally part of the same X-ray detection. Spectroscopically, we found two clusters at $z = 0.307$ ($n_z = 8$) and $z = 0.203$ ($n_z = 6$), which we designate WARP J1746.3+6849E and WARP J1746.3+6849W, respectively. We also detected a broad-line AGN with $z = 0.3058$ in the cluster (at radius $2.5'$ from the emission centroid). Subtracting the flux of this AGN and other contaminating point sources reduces the flux of the two clusters by 30%. Using aperture photometry, we estimate that 70% of the remaining flux is due to WARP J1746.3+6849W.

WARP J1930.5+7403W.—This source was originally detected as one large low surface brightness source. The eastern part has a significant fraction of flux from a QSO at $z = 1.26$ and has been discarded. The western part is probably a cluster ($z = 0.289$ for $n_z = 2$). From aperture photometry, we estimate the total flux to be 9×10^{-14} ergs cm^{-2} s^{-1}.

WARP J1941.2+7709E.—This source was originally detected as one large low surface brightness source. The western part is likely noise and point sources. The eastern part is X-ray extended,

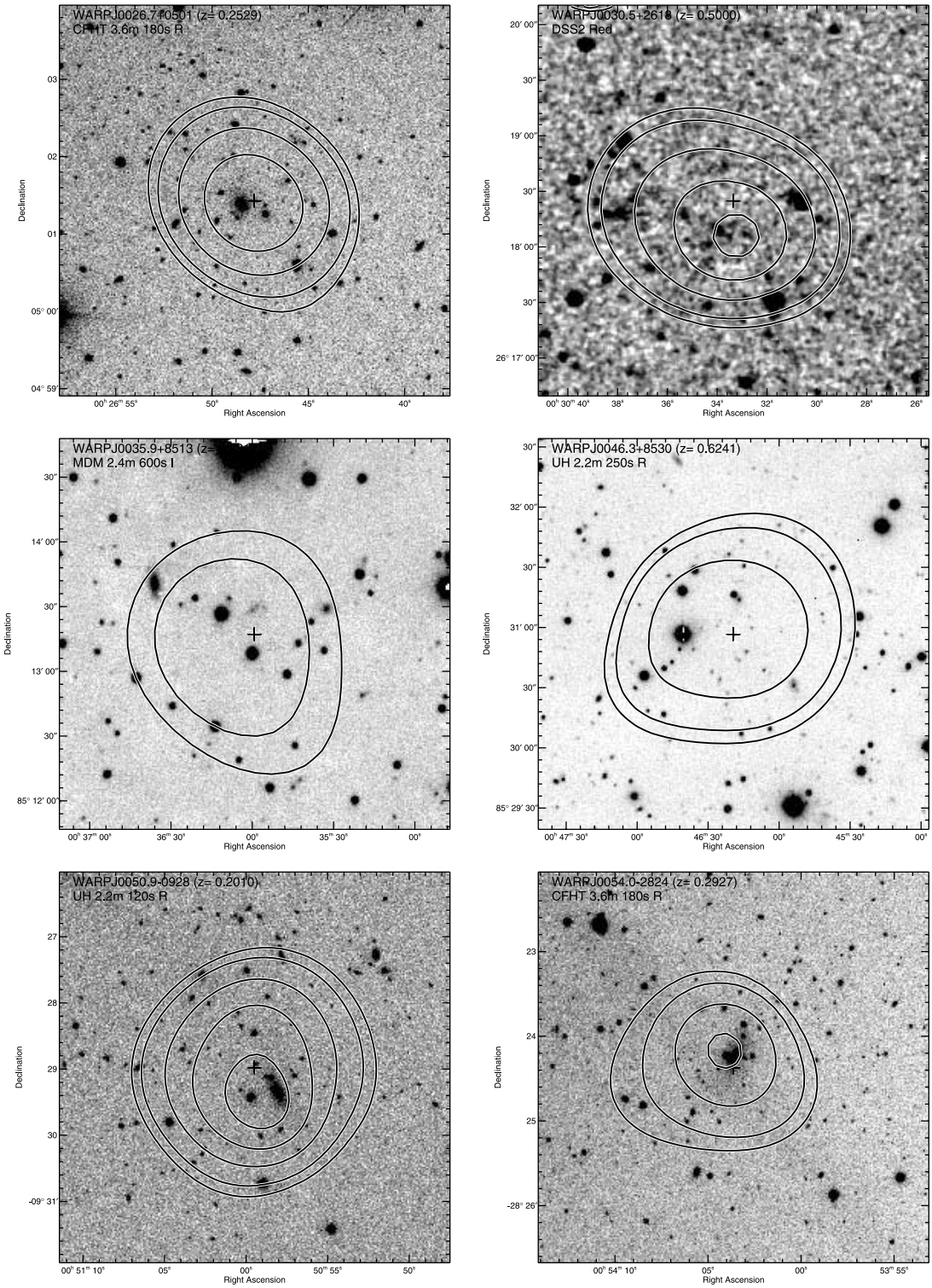

FIG. 2.—Observed 0.5–2.0 keV *ROSAT* PSPC emission contours for each cluster overlaid on an optical image (usually CCD images but with a few DSS images). Each image is 1.5 Mpc across at the cluster redshift (assuming $q_0 = 0.5$ and $H_0 = 50$ km s^{-1} Mpc^{-1}). The X-ray contours were adaptively smoothed to a minimum SNR of 3. The upper left of each image contains the cluster name along with the telescope, exposure time, and bandpass of the optical image.

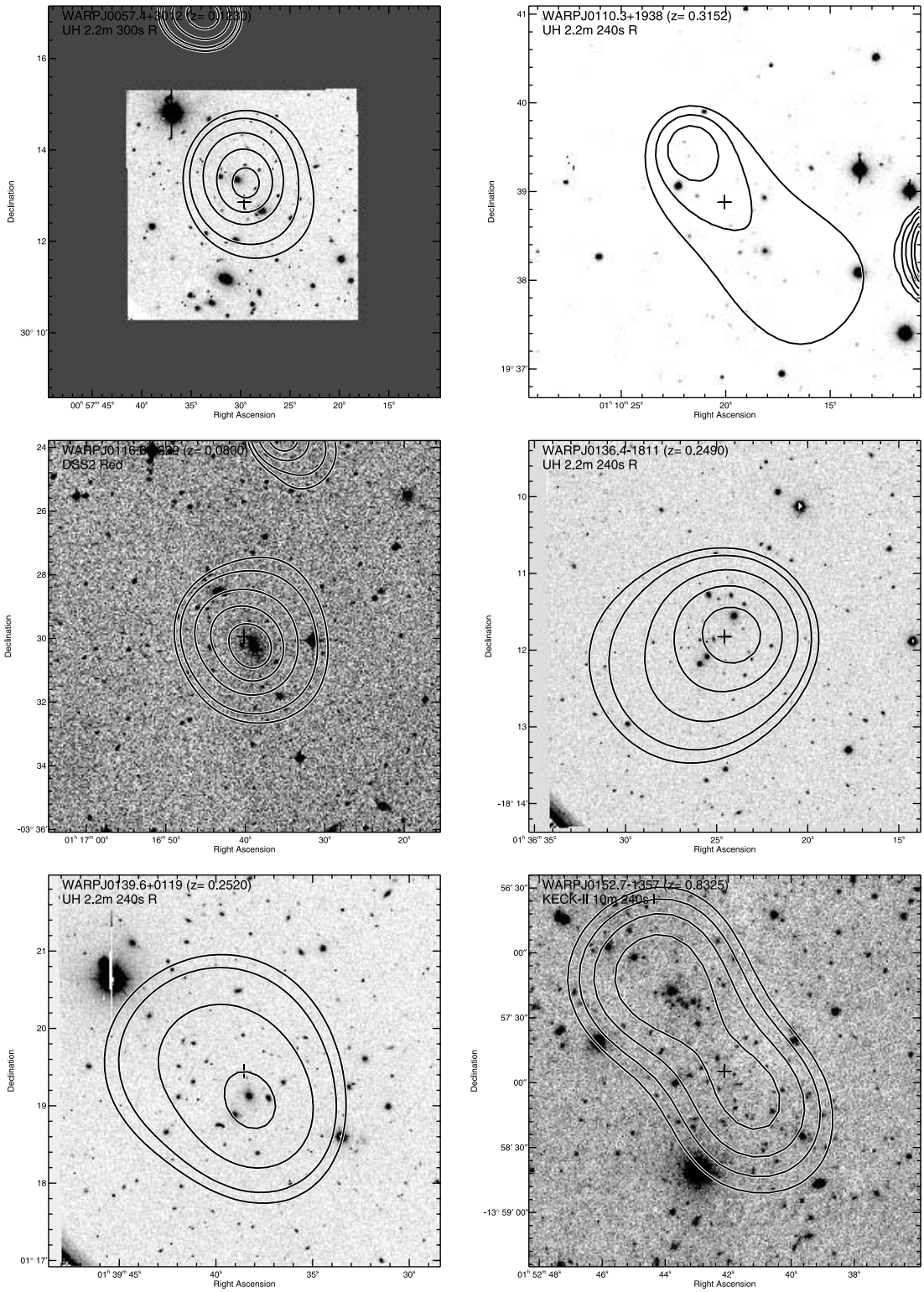

FIG. 2.—*Continued*

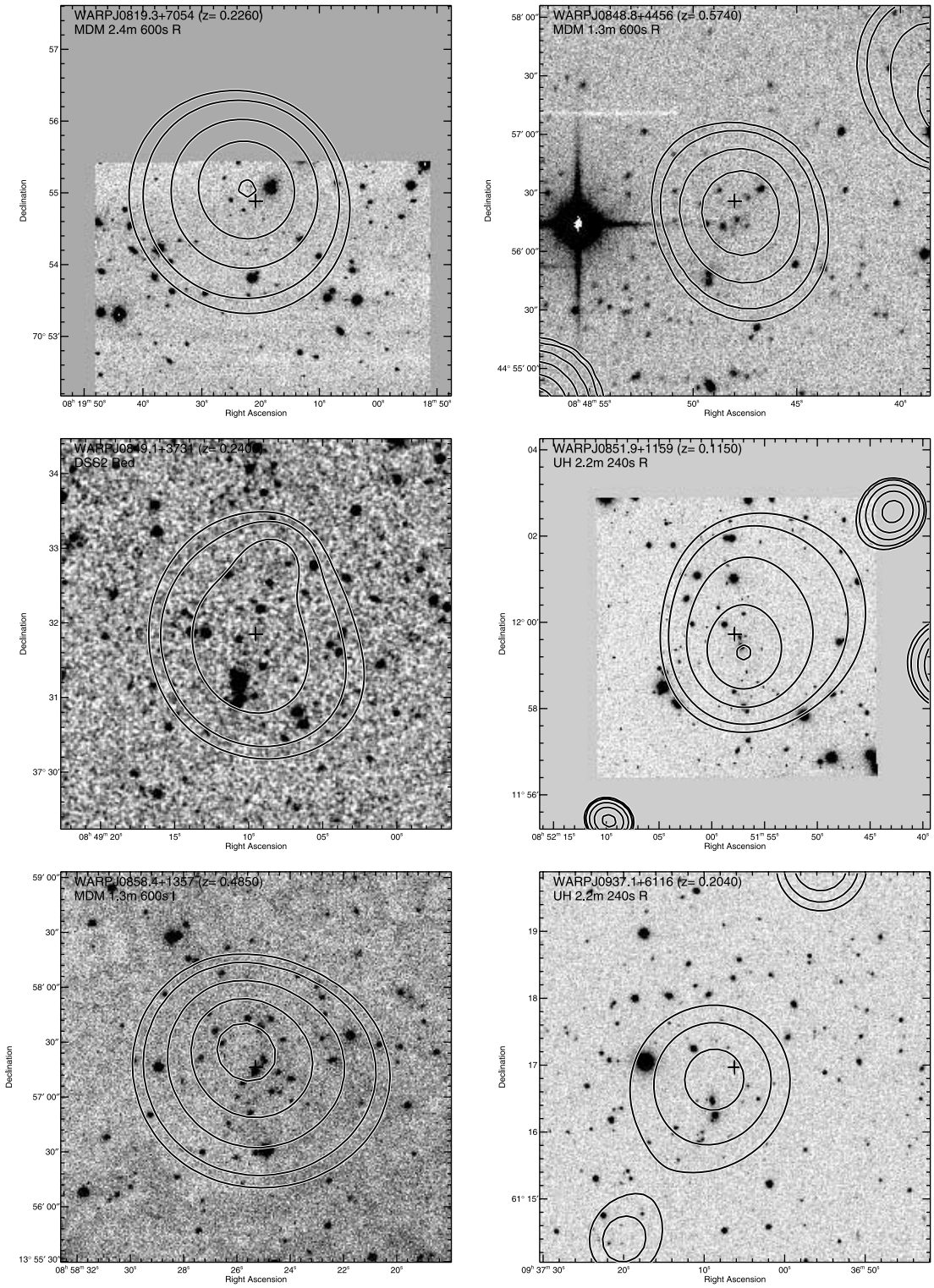

FIG. 2.—*Continued*

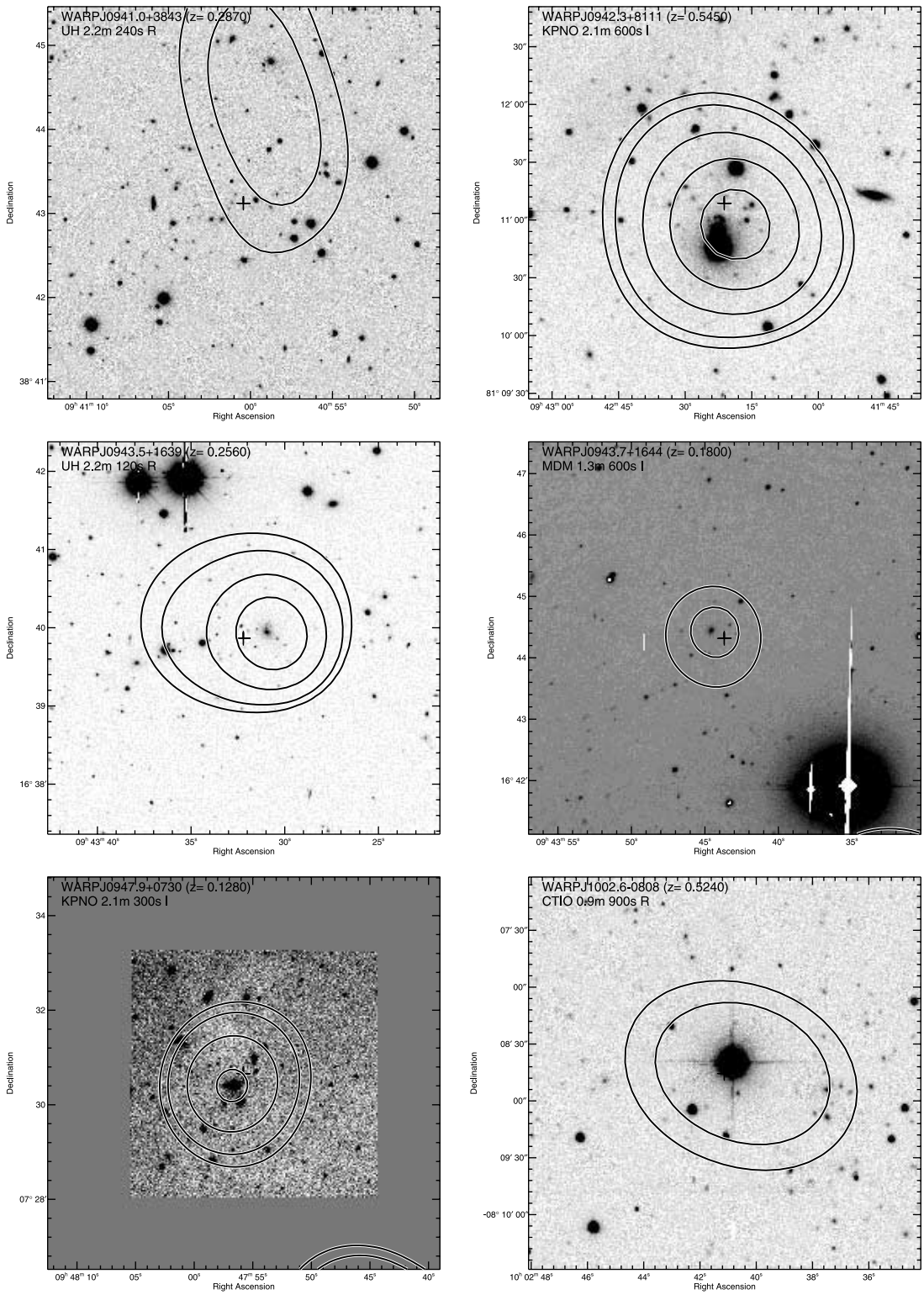

FIG. 2.—*Continued*

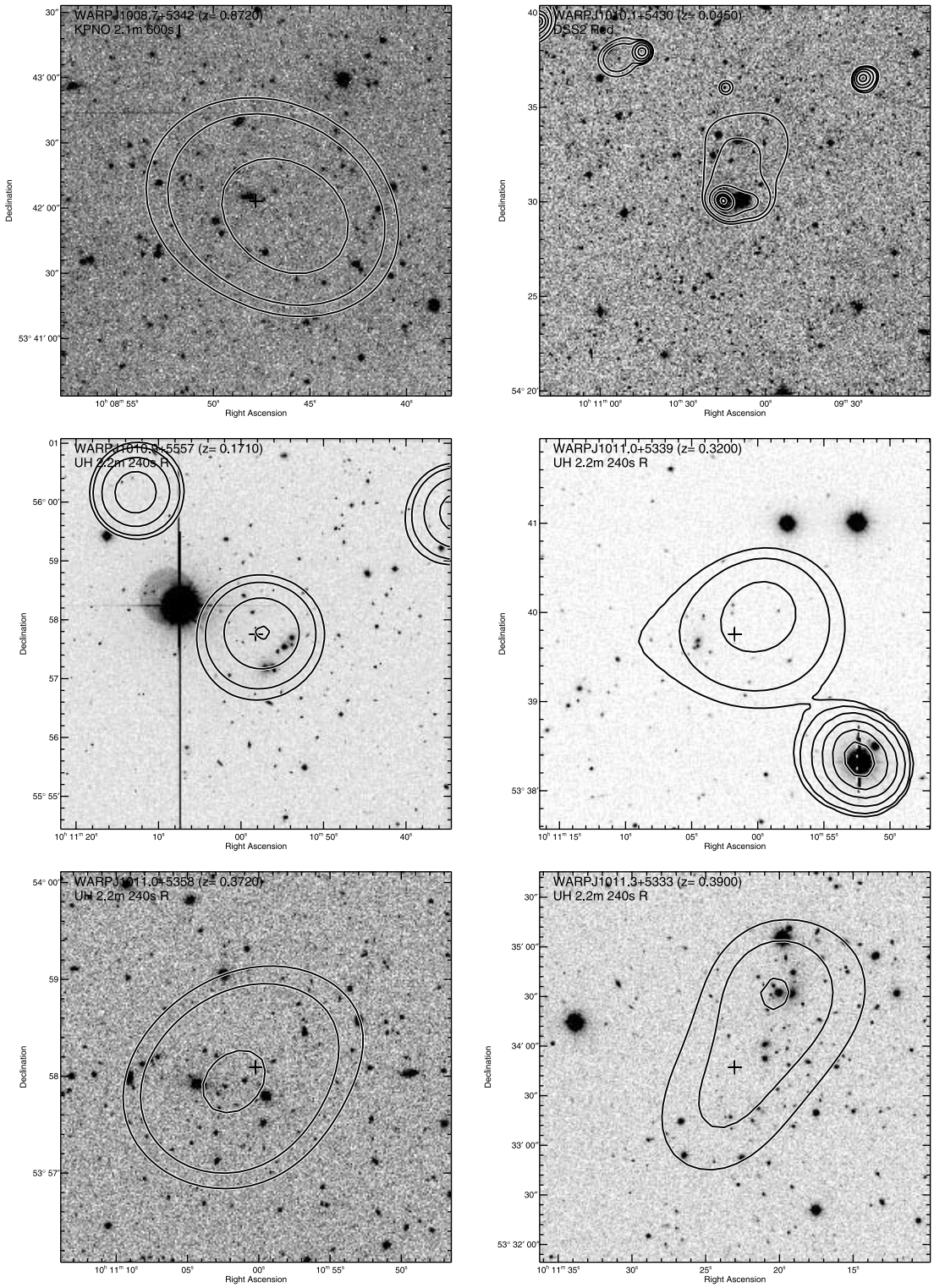

FIG. 2.—*Continued*

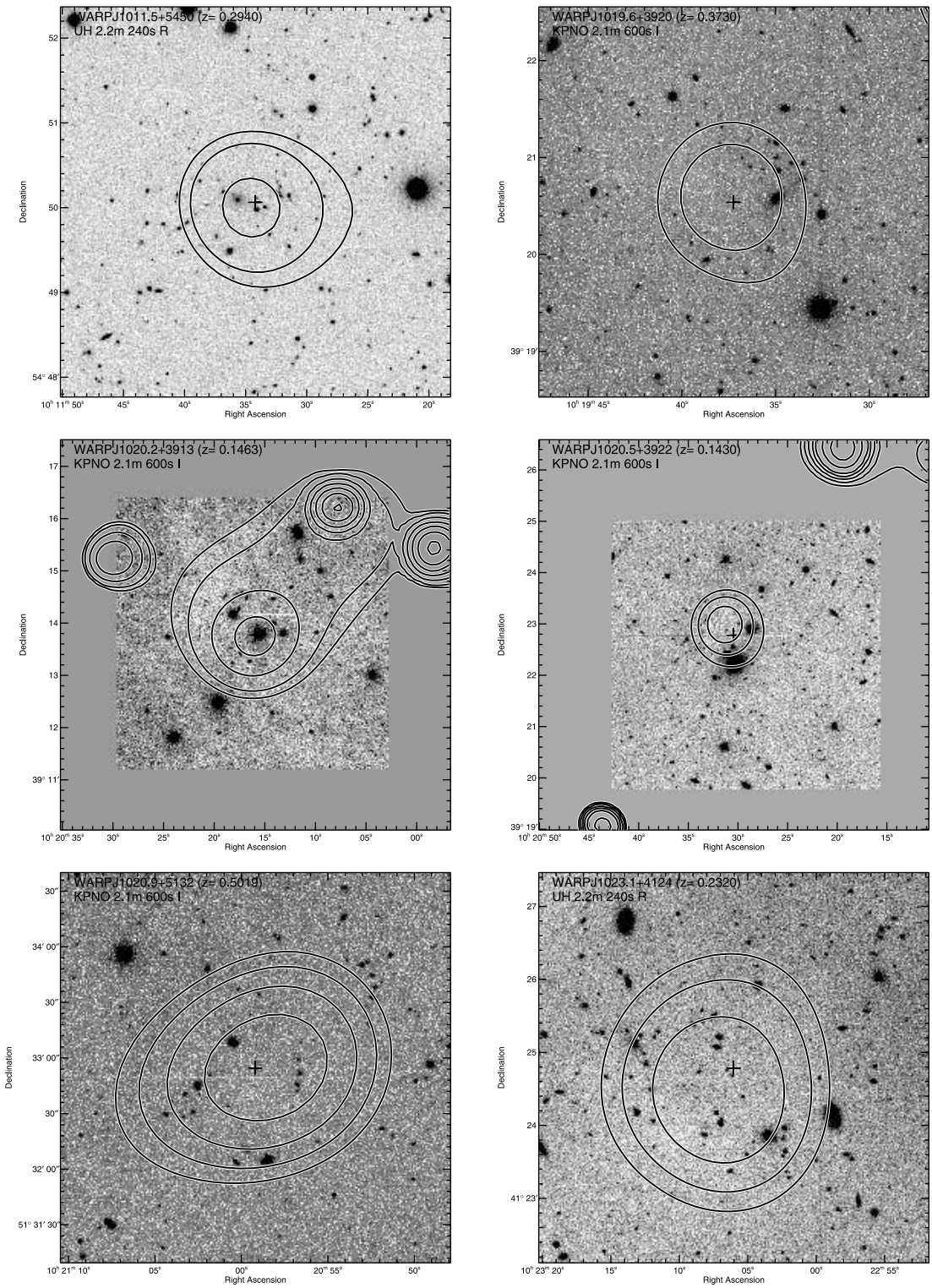

FIG. 2.—*Continued*

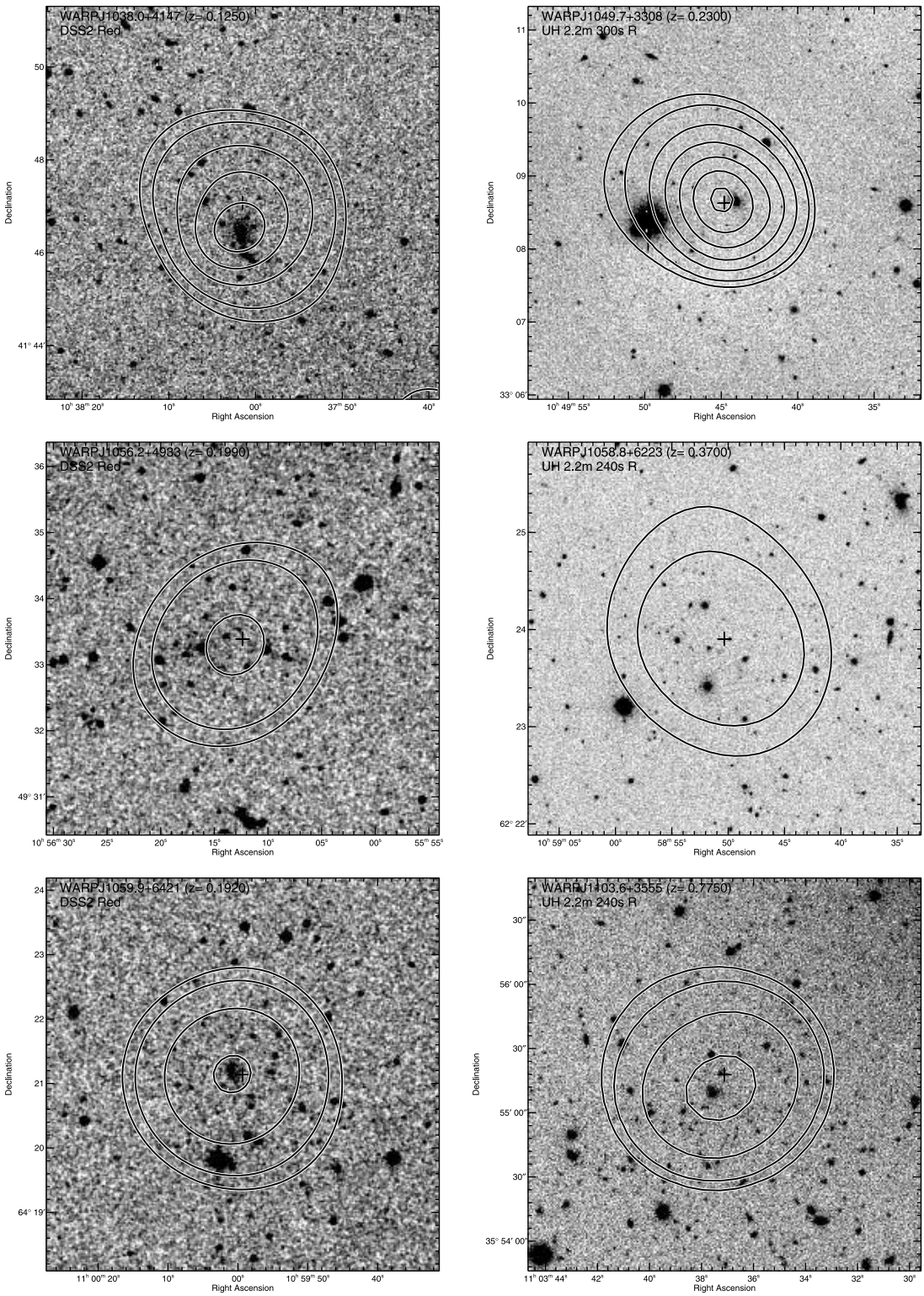

FIG. 2.—*Continued*

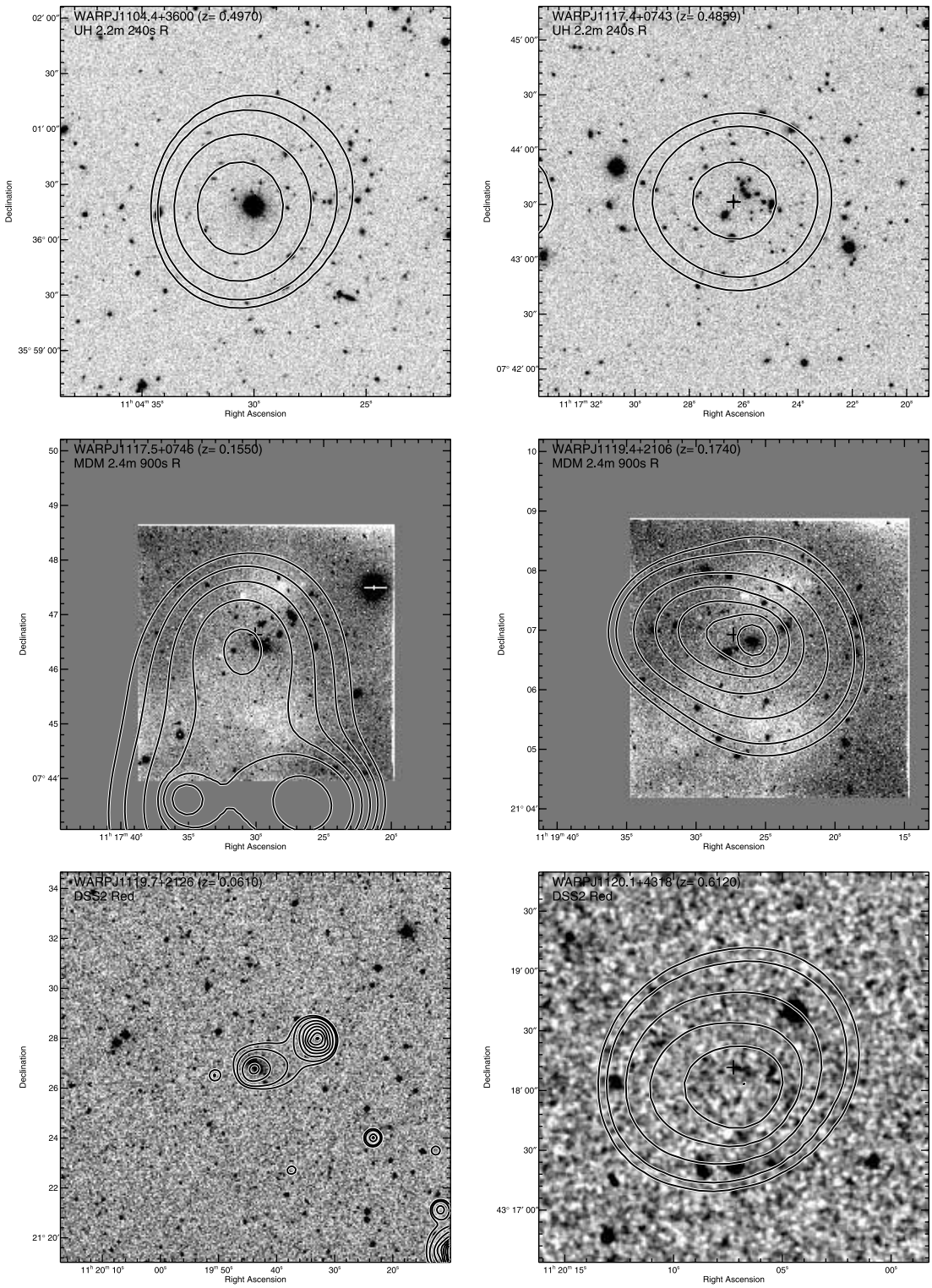

FIG. 2.—*Continued*

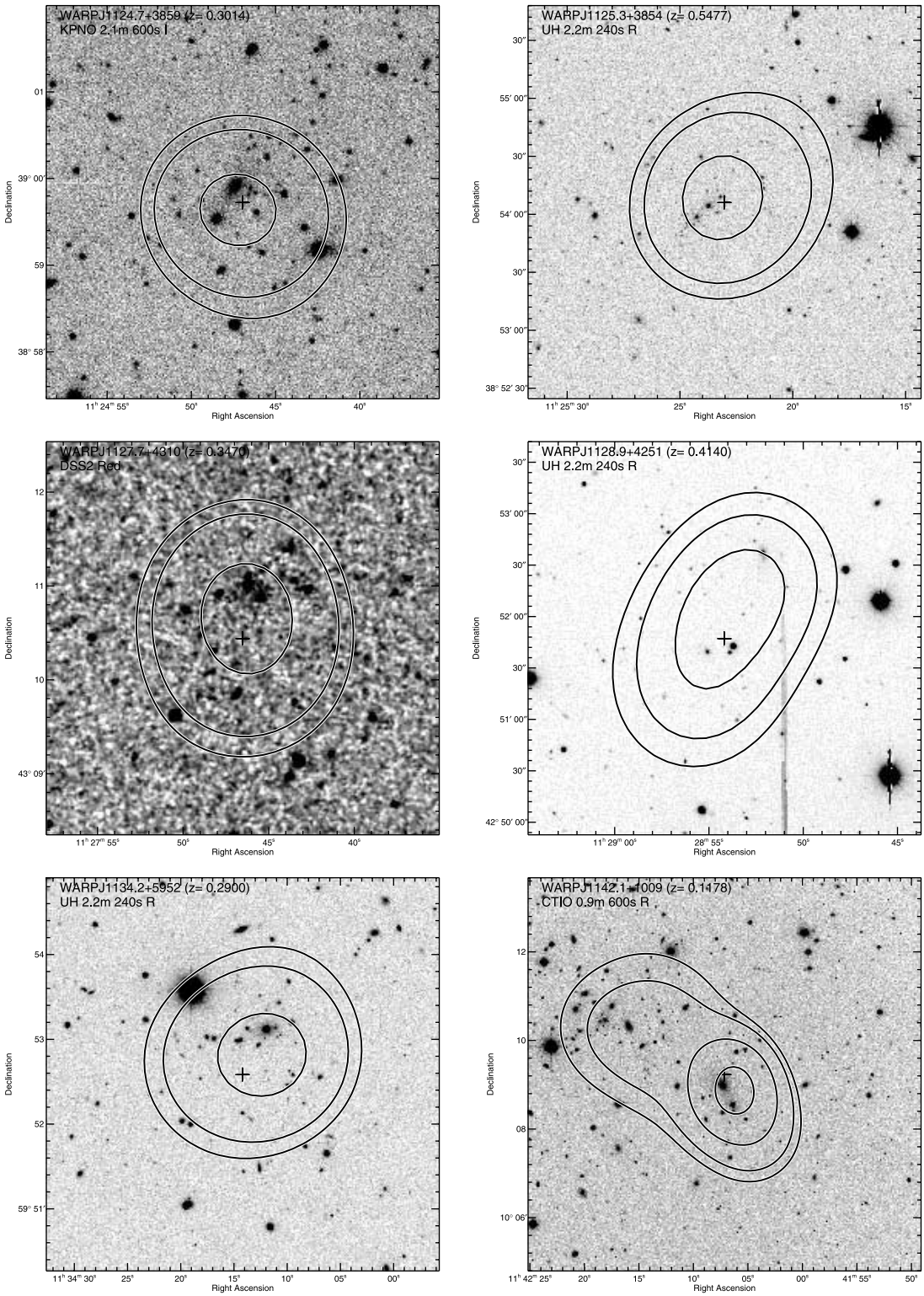

FIG. 2.—*Continued*

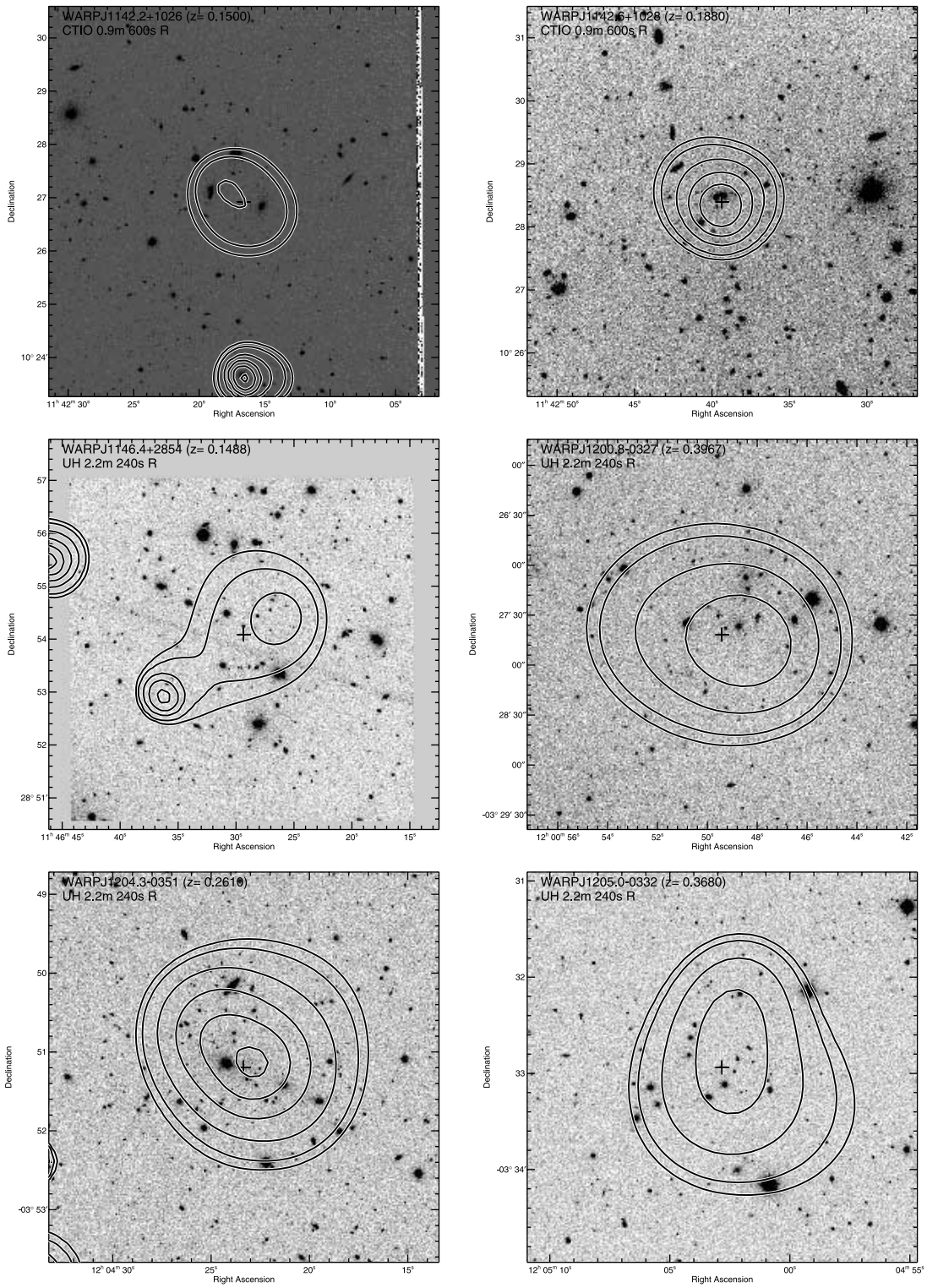

FIG. 2.—*Continued*

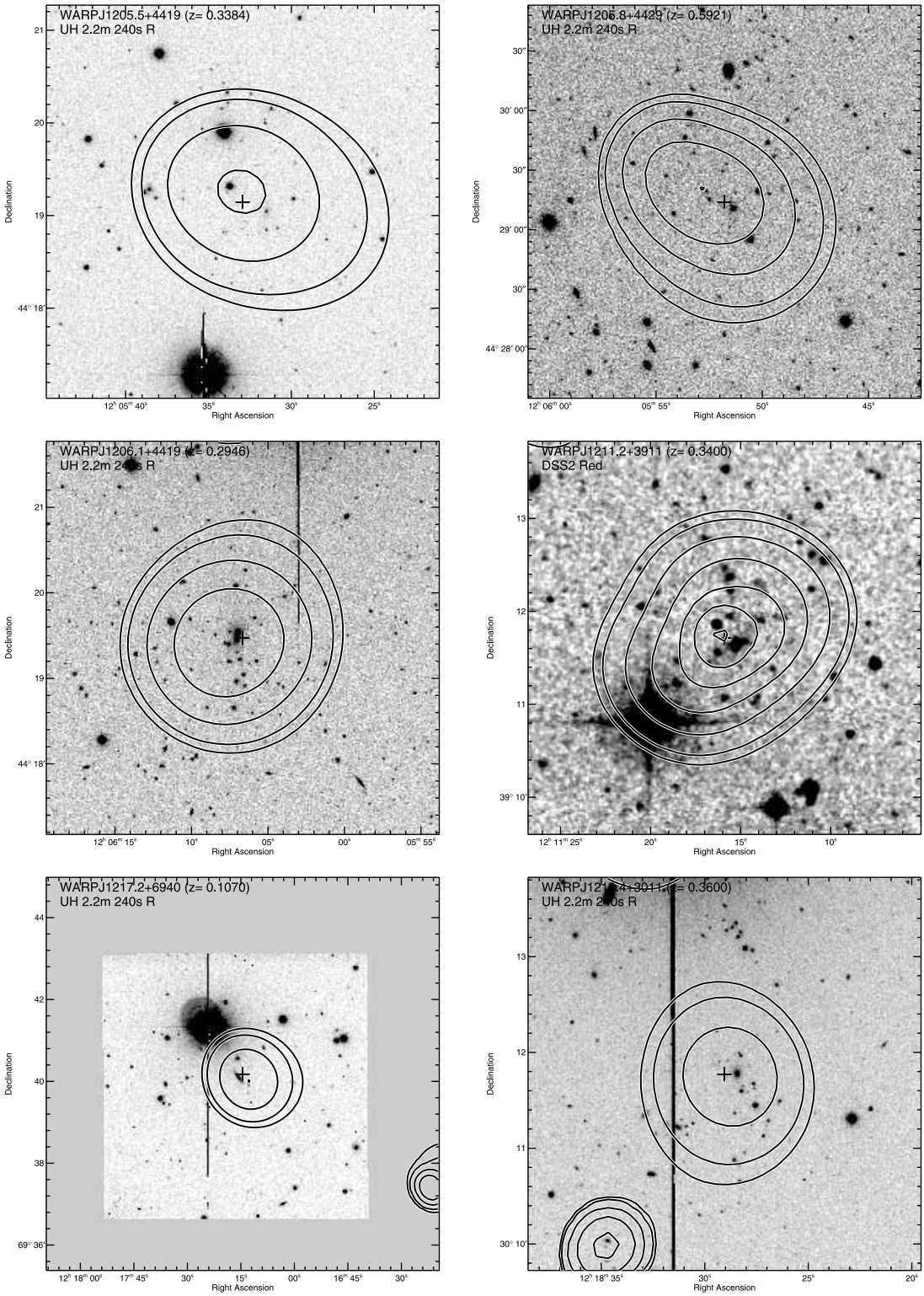

FIG. 2.—*Continued*

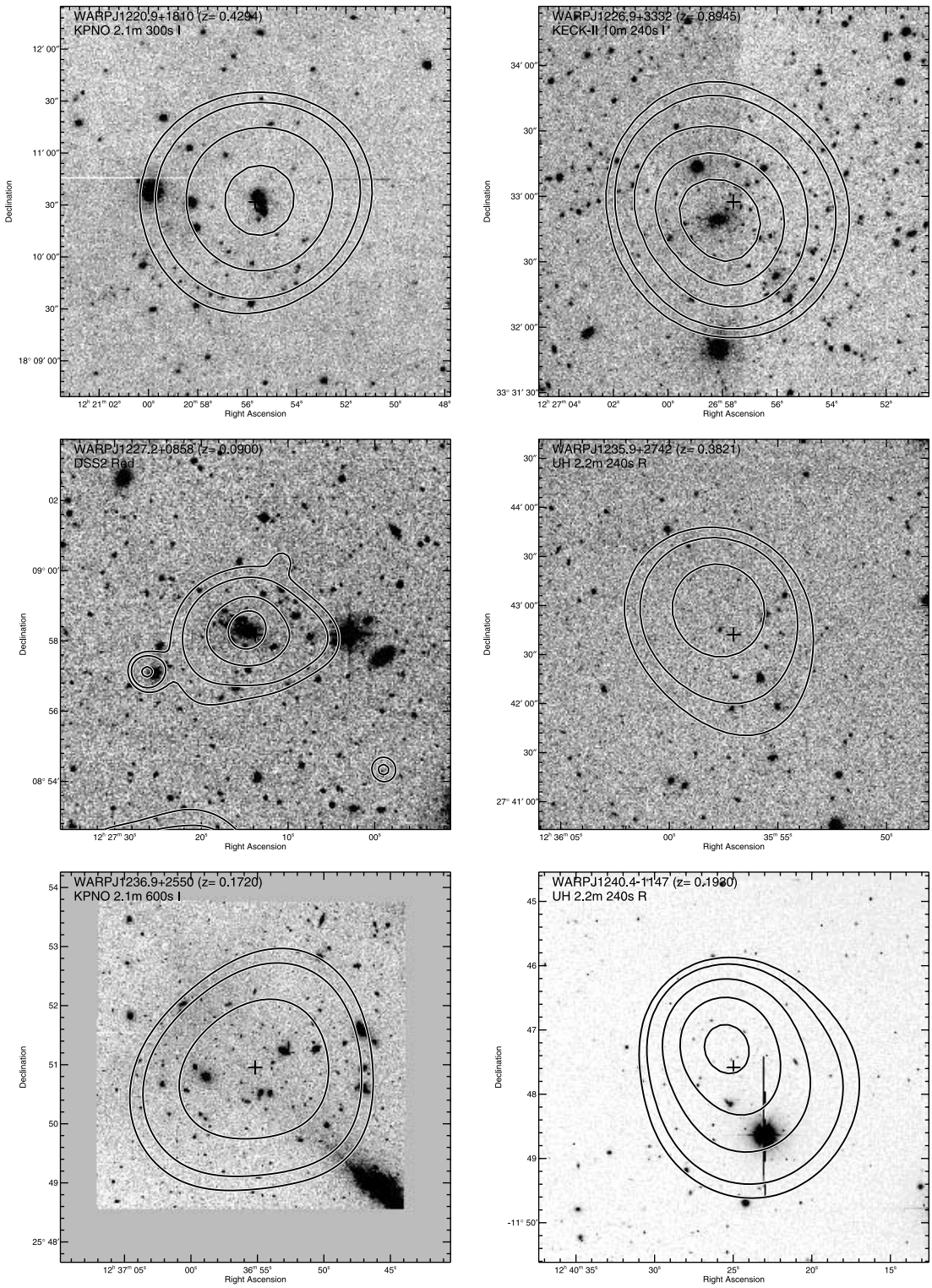

FIG. 2.—*Continued*

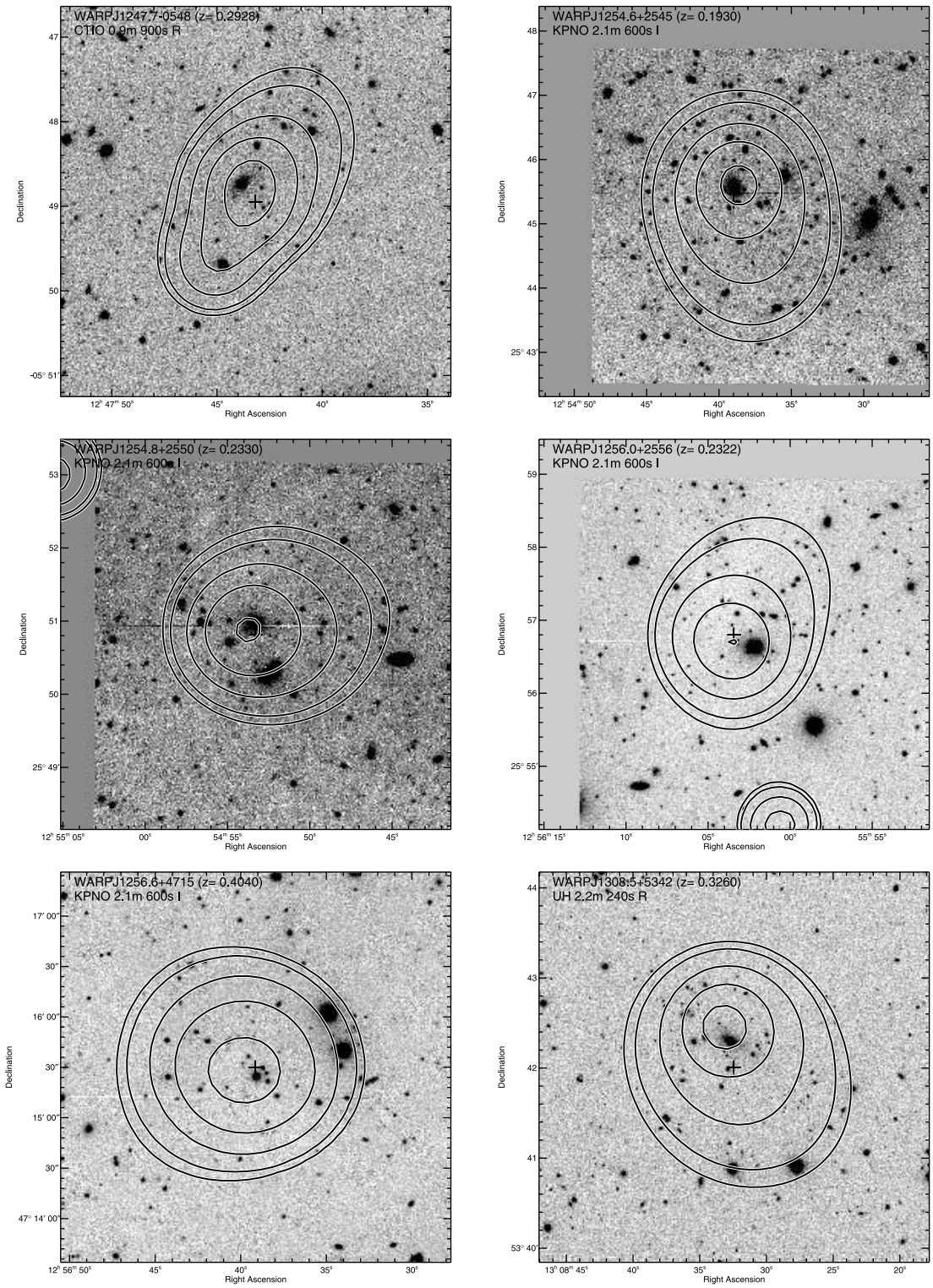

FIG. 2.—*Continued*

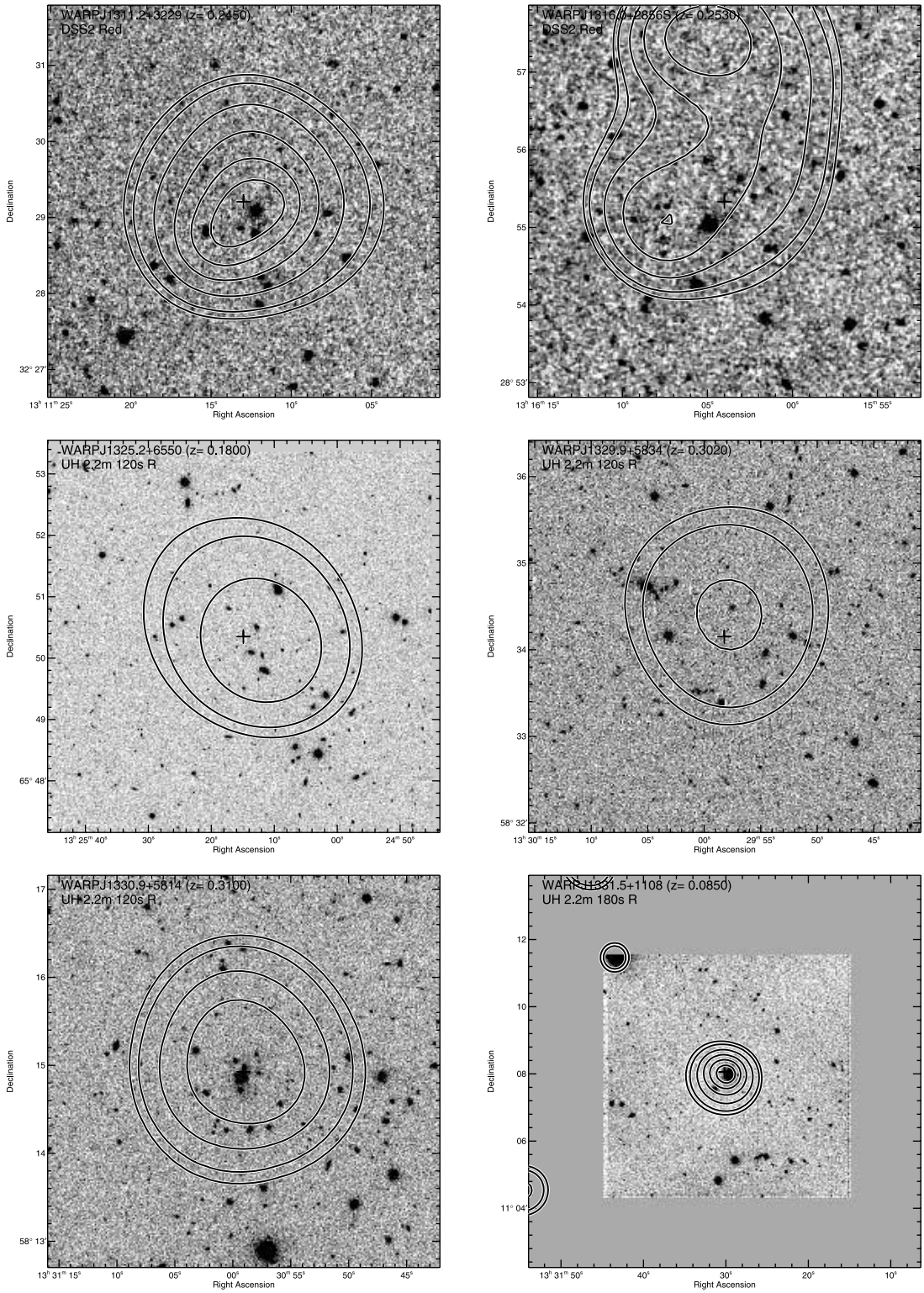

FIG. 2.—*Continued*

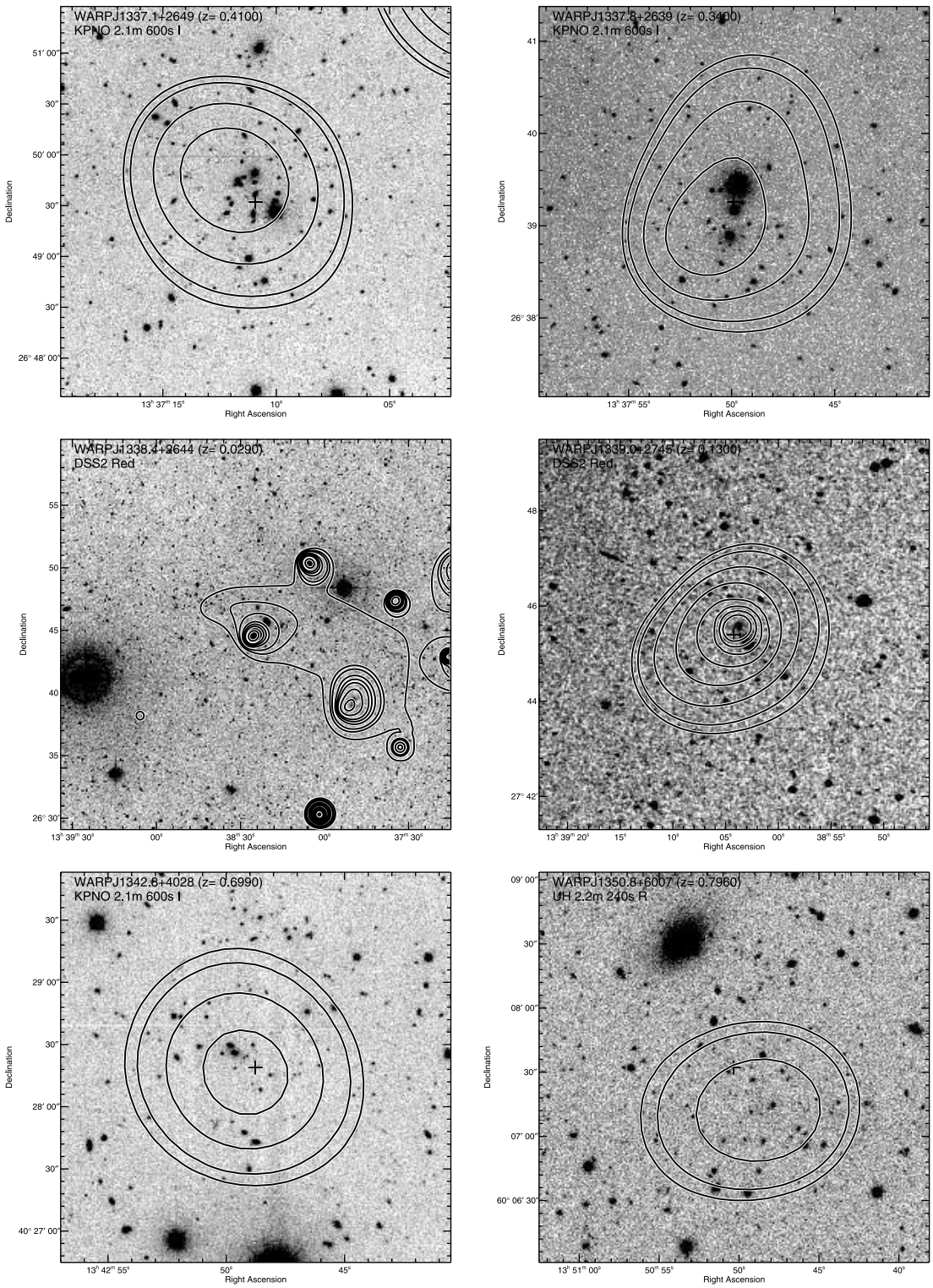

FIG. 2.—*Continued*

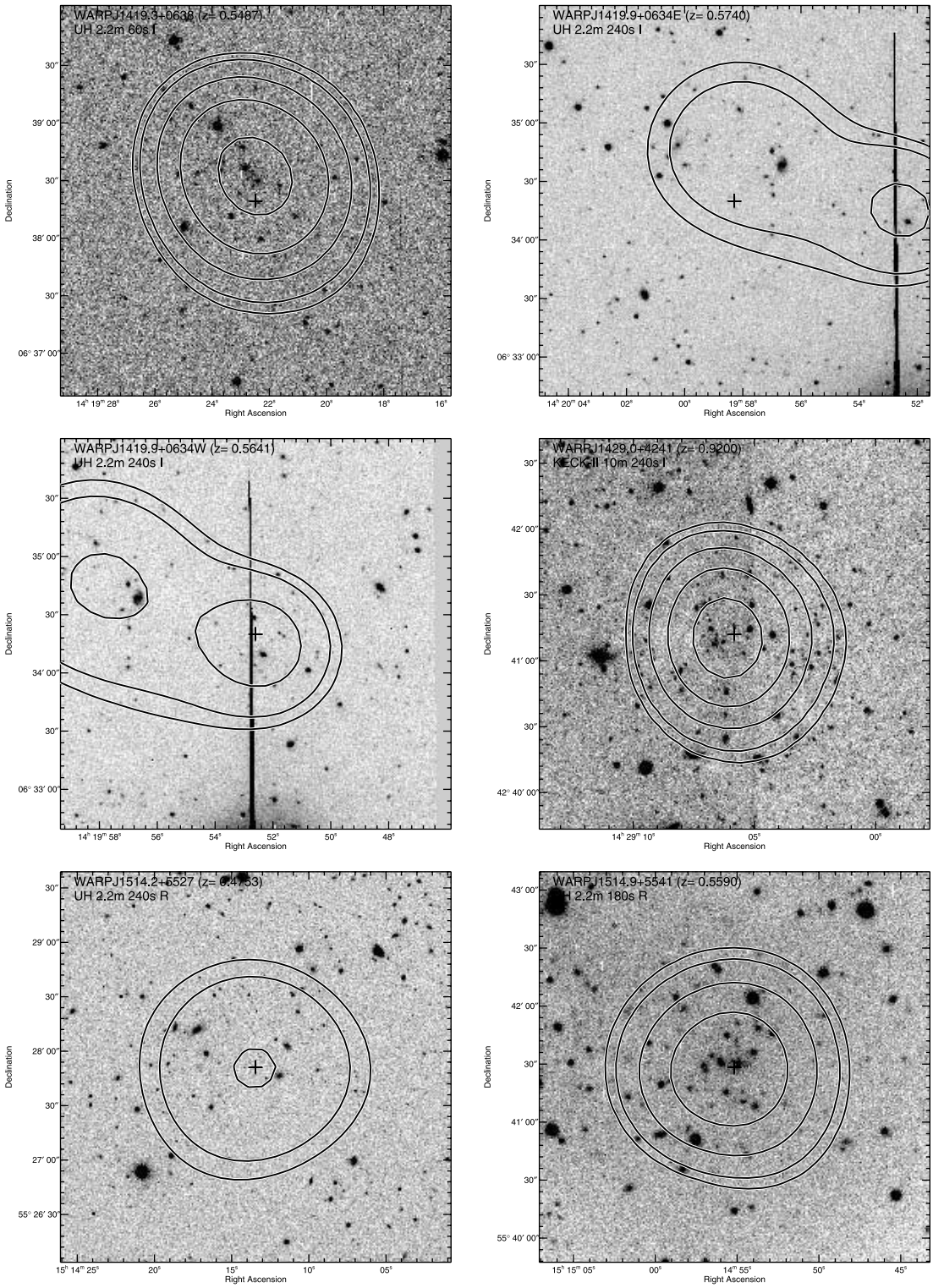

FIG. 2.—*Continued*

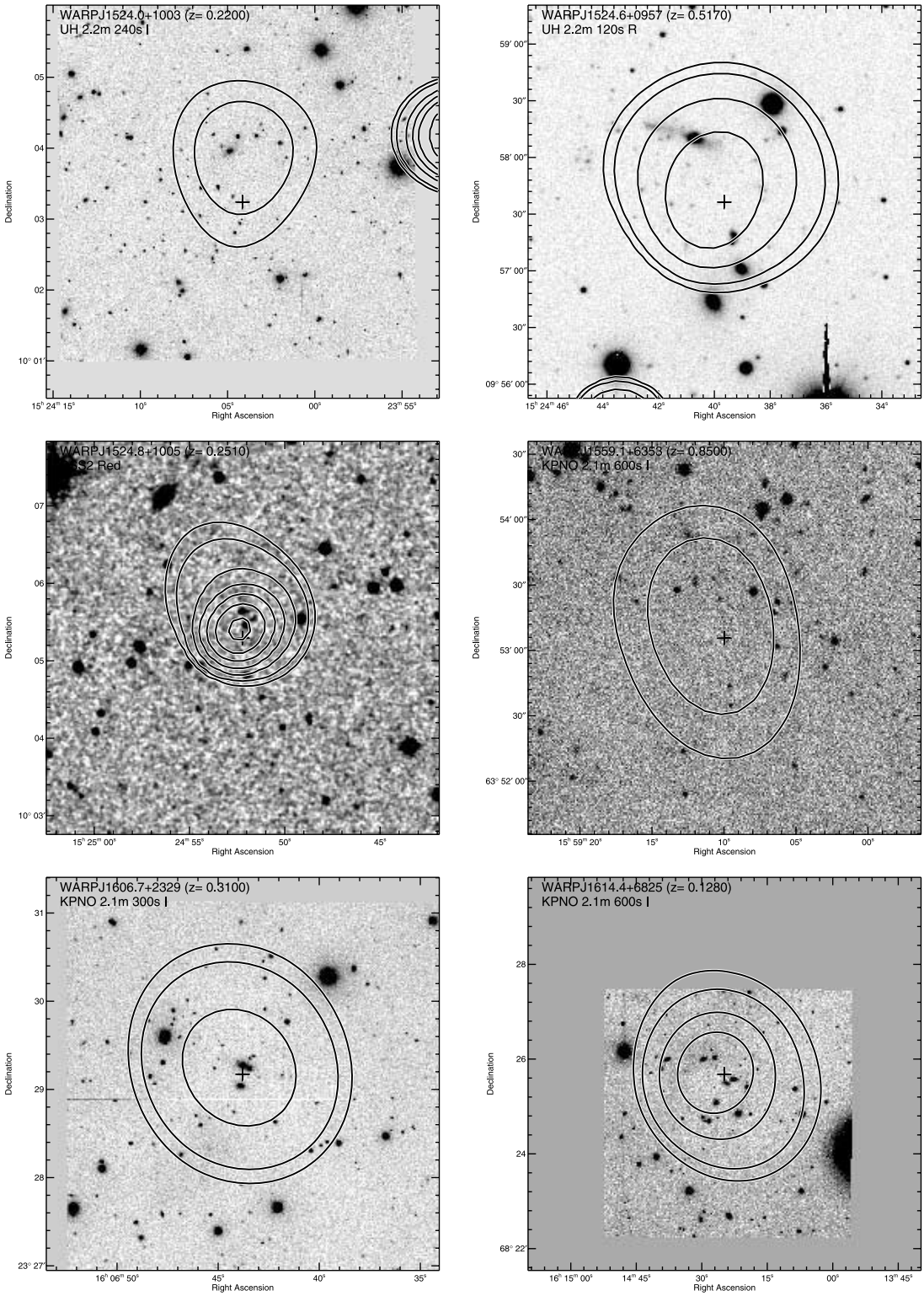

FIG. 2.—*Continued*

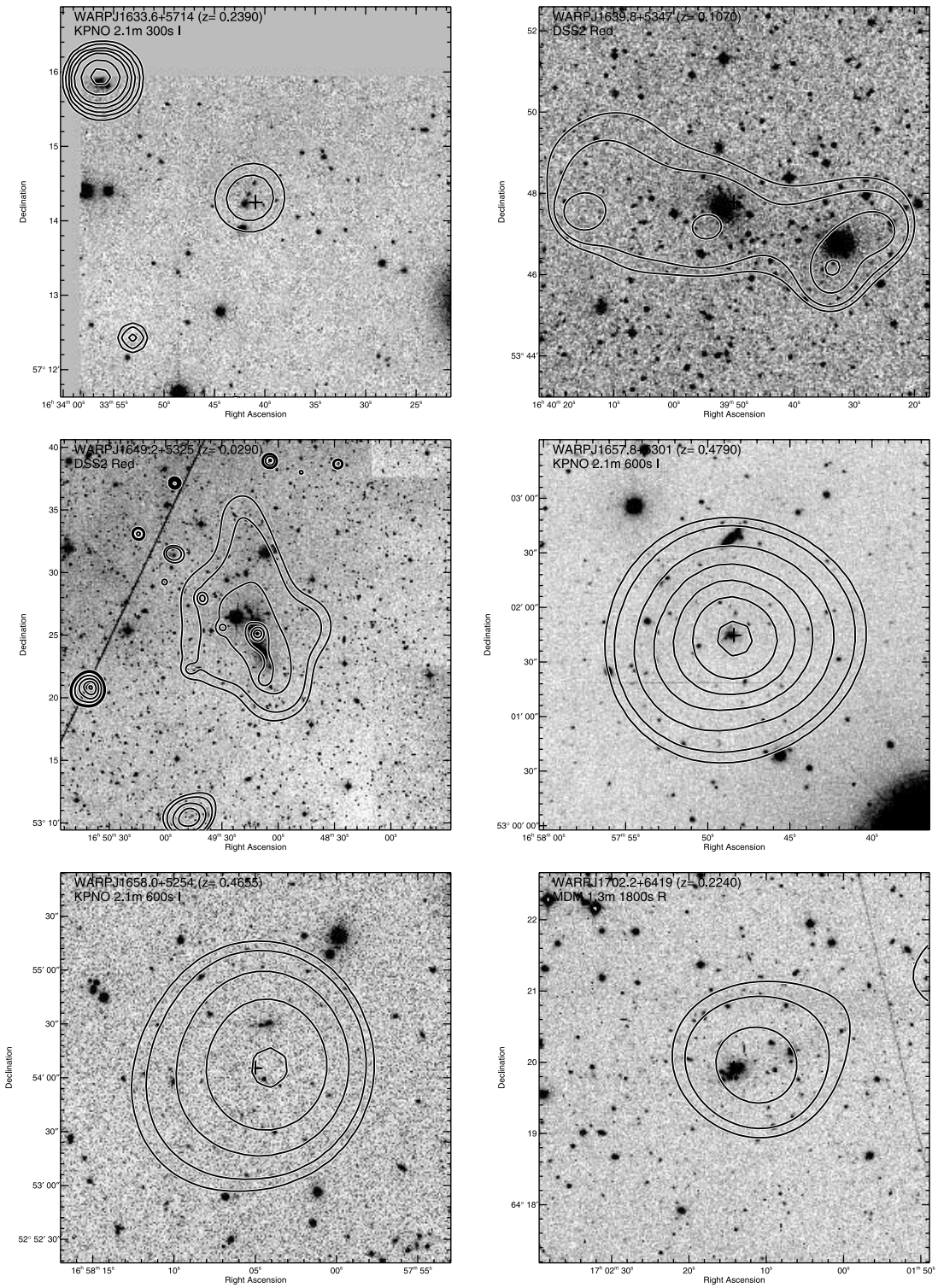

FIG. 2.—*Continued*

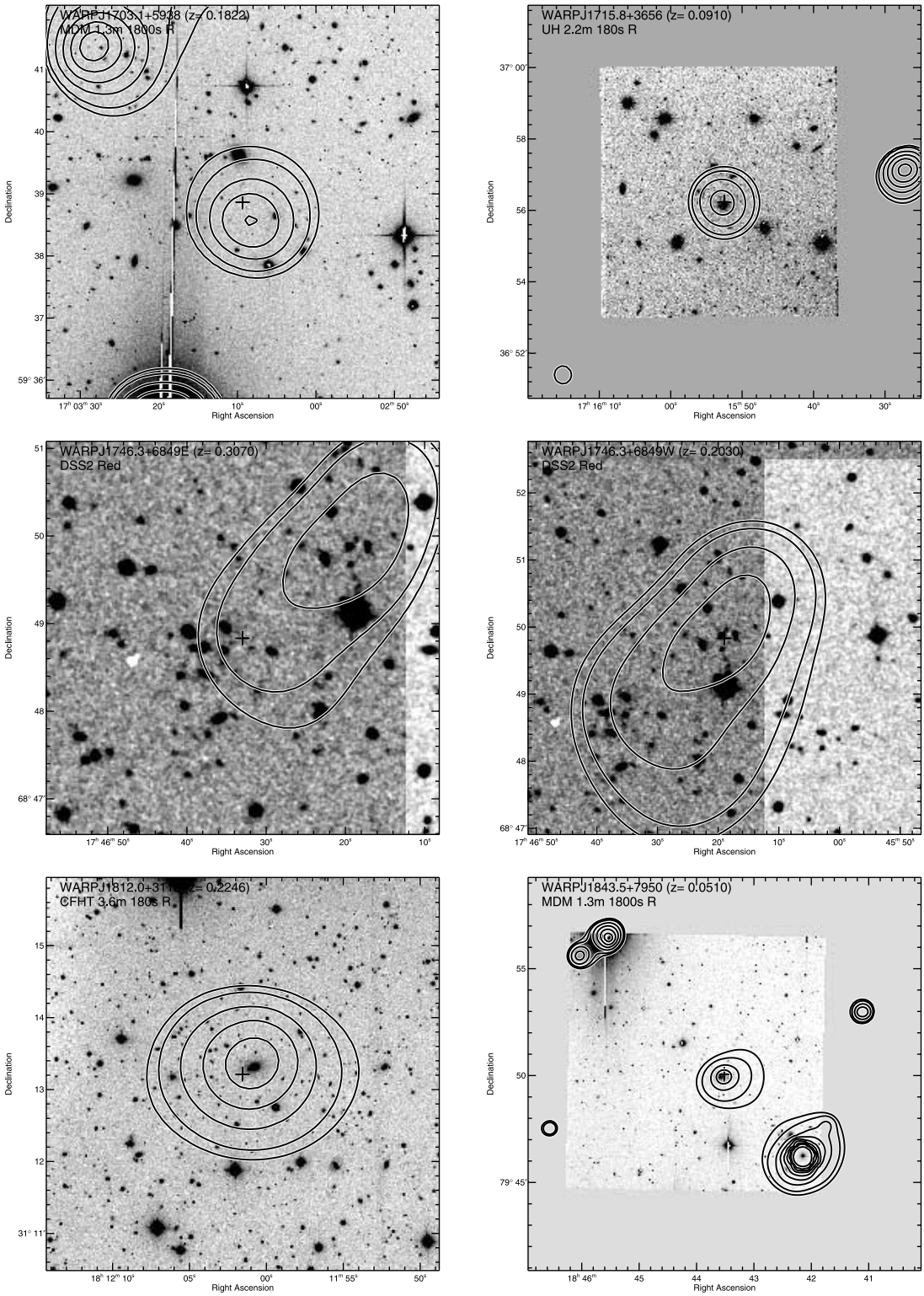

FIG. 2.—*Continued*

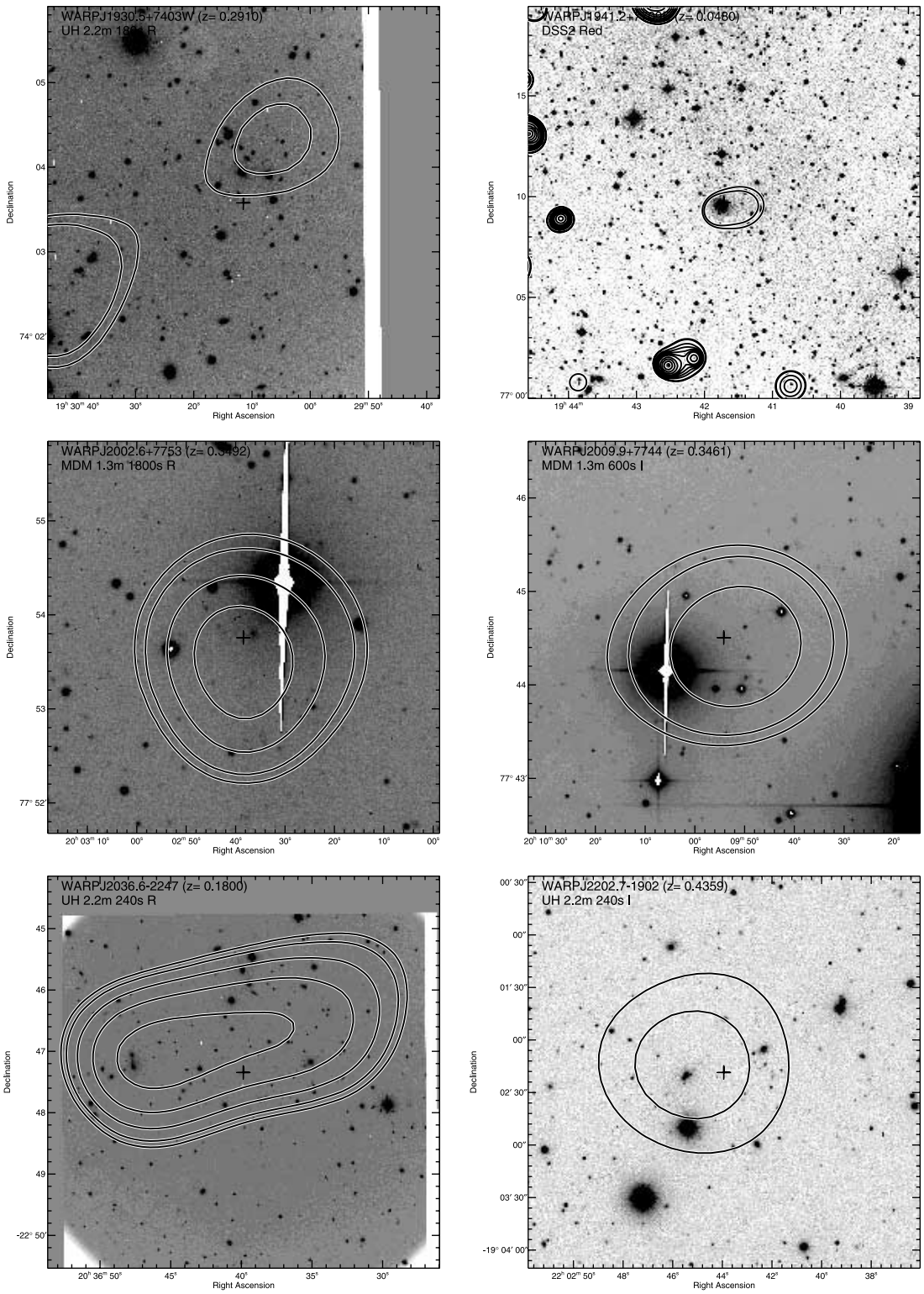

FIG. 2.—*Continued*

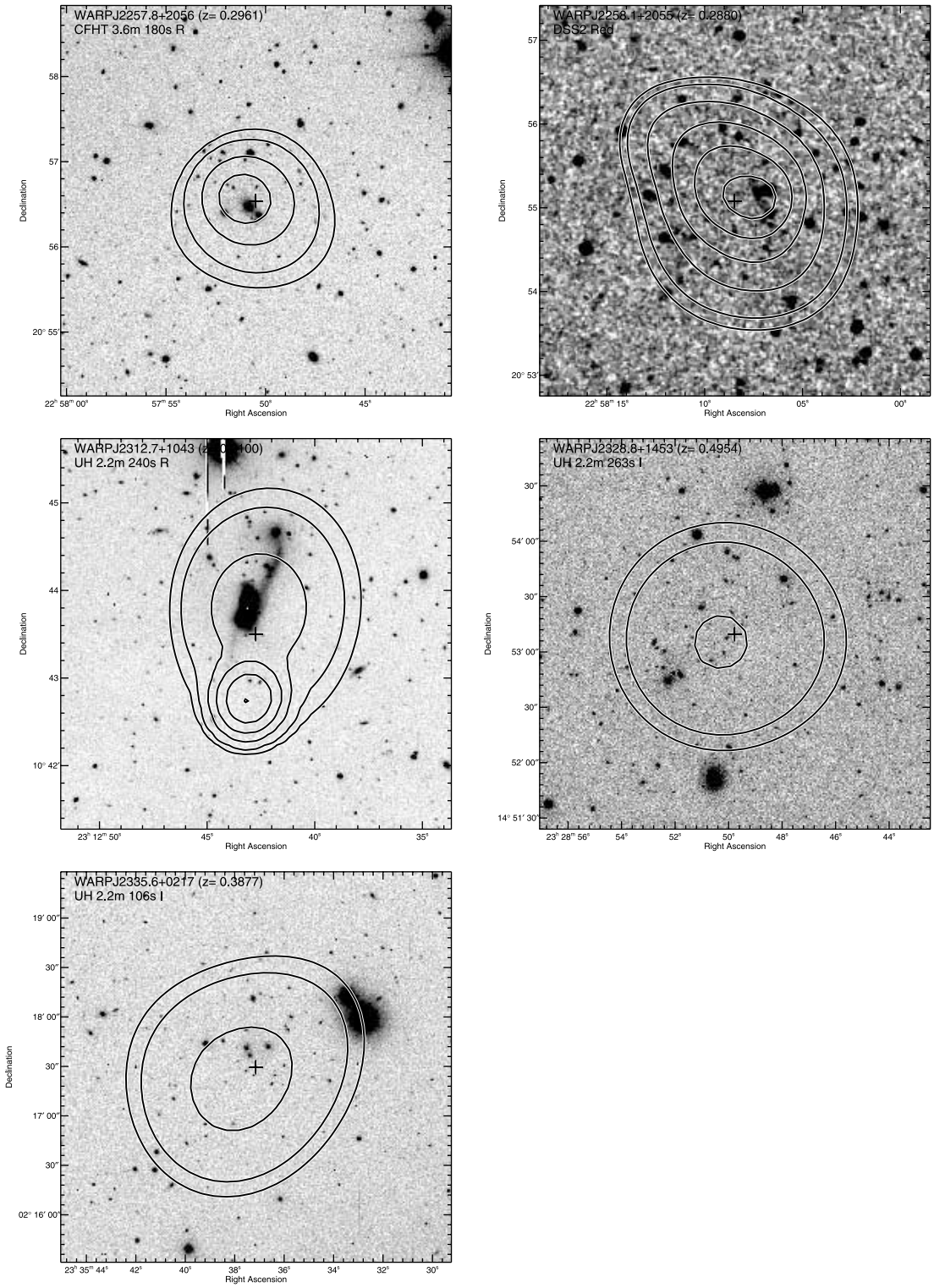

FIG. 2.—*Continued*

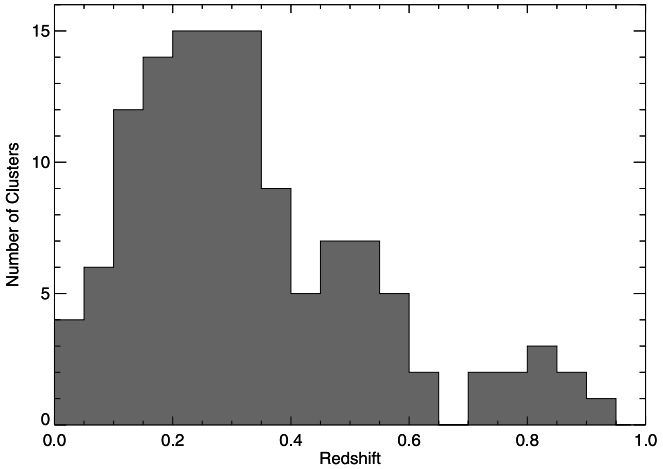

FIG. 3.—Redshift distribution of the cluster sample. The distribution has a median of $z = 0.29$ with minimum and maximum values of 0.029 and 0.92, respectively.

and we have $z = 0.048$ ($n_z = 2$). From aperture photometry, we estimate the total flux to be 2.5×10^{-14} ergs cm^{-2} s^{-1}, well below our limit.

WARP J2036.6−2247.—This source is a low surface brightness double cluster that is difficult to distinguish from noise and point sources and near the limit of our detectability. We do not have a redshift for this cluster.

4. COMPARISON WITH OTHER SURVEYS AND FLUX MEASUREMENTS

Several other groups have undertaken *ROSAT* PSPC serendipitous surveys similar to WARPS. All use many of the same *ROSAT* PSPC fields, so a significant number of shared objects is to be expected. Table 4 lists many of the WARPS clusters found in other surveys (including non–X-ray surveys). In this section, we compare our detection, redshifts, and fluxes with published catalogs from the 160SD Survey, SHARC, and RIXOS. Since they have not published a catalog, we cannot compare with the RDCS. Table 5 and Figure 5 summarize the flux comparison between WARPS and these surveys.

4.1. *The 160SD Survey*

The CfA 160 deg^2 (160SD) survey produced a catalog of 201 clusters (Vikhlinin et al. 1998) detected in 647 *ROSAT* PSPC fields. They employed a wavelet decomposition algorithm to detect X-ray sources in an annular region of 2.5′–17′ in each field. Their *ROSAT* field selection and subsequent optical follow-up program was substantially similar to WARPS, but they used mostly photometric redshifts. The 160SD survey group subsequently updated and revised the catalog with spectroscopic redshifts (Mullis et al. 2003). The area of the 160SD sample is a strong function of flux. Although they cover 160 deg^2 at high fluxes, their sky coverage drops for low fluxes (see Table 5 in Vikhlinin et al. 1998). The median flux of the survey is 1.2×10^{-13} ergs cm^{-2} s^{-1} with an effective minimum of 3.7×10^{-14} ergs cm^{-2} s^{-1}.

We find 157 *ROSAT* fields and 44 clusters in common between the 160SD survey and WARPS-II catalogs. We split two of the 44 common clusters into separate sources based on redshift information. We ignore these clusters in the following flux and redshift comparisons. The spectroscopic redshifts in Mullis et al. (2003) and ours agree to within a few percent for all sources. Figure 5 shows the ratio of 160SD fluxes to WARPS-II flux as a function of redshift. Overall, the fluxes agree fairly well with

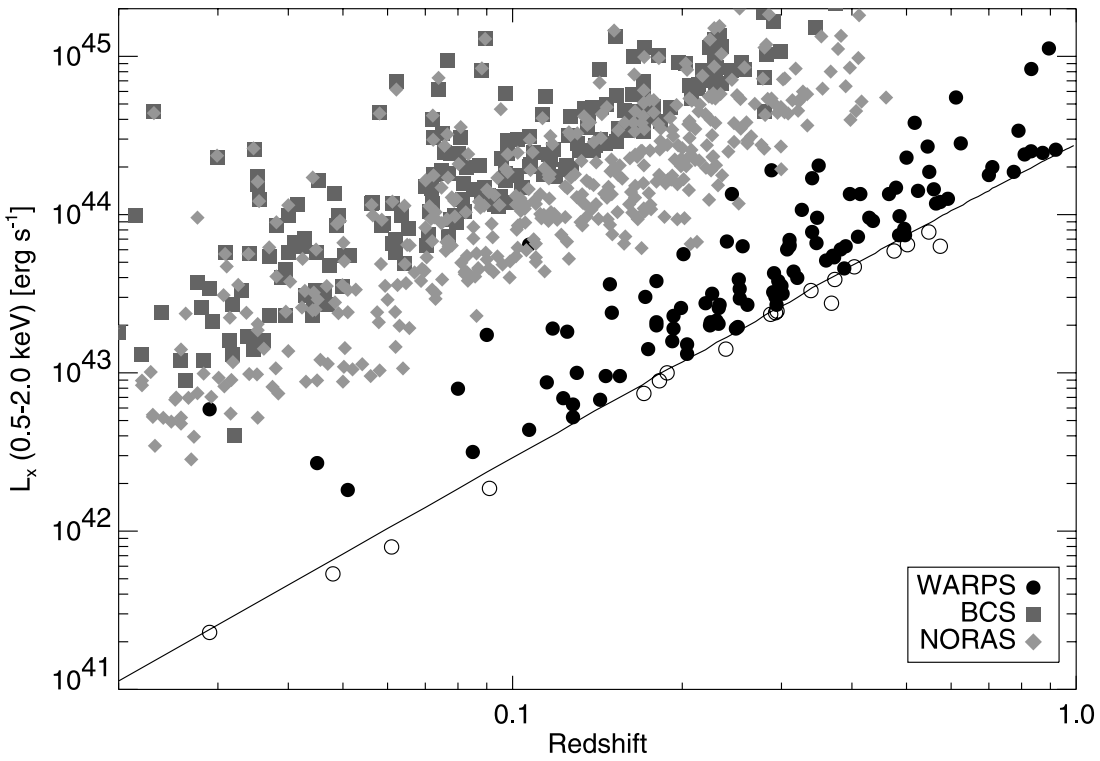

FIG. 4.—X-ray luminosity and redshift distribution of the sample (assuming $q_0 = 0.5$ and $H_0 = 50$ km s^{-1} Mpc^{-1}). The solid line indicates the flux limit of 6.5×10^{-14} ergs cm^{-2} s^{-1}. WARPS clusters are marked by circles. Clusters marked with open circles are below the flux limit for inclusion in the statistical sample. For comparison, we also plot clusters from the BCS (Ebeling et al. 1998) and NORAS (Böhringer et al. 2000) X-ray surveys based on *ROSAT* All-Sky Survey data using squares and diamonds, respectively.

TABLE 5
FLUX COMPARISONS

Catalog	$\langle f_x(\text{Catalog})/f_x(\text{WARPS})\rangle$	1 σ	N	Comments
160SD	0.94	0.38	42	
160SD	0.89	0.22	41	Excluding WARP J1011.5+5450
BSHARC	1.07	0.41	9	
BSHARC	0.93	0.11	8	Excluding WARP J1142.2+1026
SSHARC	1.26	0.52	9	
SSHARC	1.02	0.17	7	Excluding WARP J1142.2+1026 and WARP J1227.2+0858
RIXOS	0.72	0.26	17	$\alpha = -1$
RIXOS	0.40	0.19	17	Fitted α

a mean and standard deviation of $f_x(160SD)/f_x(WARPS) = 0.89 \pm 0.22$, although our fluxes seem to be systematically slightly higher (see Table 5 and Fig. 5). Similarly, the core radii agree fairly well with a mean and standard deviation of $r_c(160SD)/r_c(WARPS) = 1.15 \pm 0.36$.

These flux and core radii comparisons exclude WARP J1011.5+5450, which has a flux almost a factor of 3 higher in the 160SD survey (including it would move the average flux ratio to 0.94) and a core radius over 6 times ours. WARP J1011.5+5450 is at $z = 0.294$, and the 160SD core radius of 94″ (∼500 kpc in linear size) is actually the largest they measure in the range $0.25 < z \leq 0.35$ and would be quite large for any cluster. The difference seems to be that the 160SD detection merges several blobs of emission into a single source (A. Vikhlinin 2004, private communication).

In the 157 common *ROSAT* fields, 160SD contains 26 clusters that are not in the WARPS-II catalog. However, we searched only a 3′–15′ annulus around the field center, while 160SD used a somewhat larger 2.5′–17′ annulus. Ignoring clusters outside our survey area or well below our flux limit (such as RX J0848.9+4452, the now famous $z = 1.26$ X-ray cluster first reported by Rosati et al. 1999) leaves 7 160SD clusters unaccounted for. We examined each of these clusters to determine why they were left out of the WARPS-II sample. In general, the disagreements are simply due to low SNR, different measurements of the flux near our flux limit, and possible point-source contamination and do not represent any significant problems with our detection methods or completeness. Given the ≈20% scatter in the flux ratio (see Table 5), probably largely due to different procedures in the extrapolation from detected to total flux, it is not surprising that some clusters detected just above the flux limit of each survey fall below the flux limit of the other survey. Below we give detailed explanations for each of these 160SD clusters (which are listed by their names in Mullis et al. 2003 and original numbers in Vikhlinin et al. 1998).

RXJ0124.5+0400 (*no. 11*).—We identified this source as extended in our processing but with a flux of 5.0×10^{14} ergs cm^{-2} s^{-1}, which is well below our flux limit. A poor-quality image we

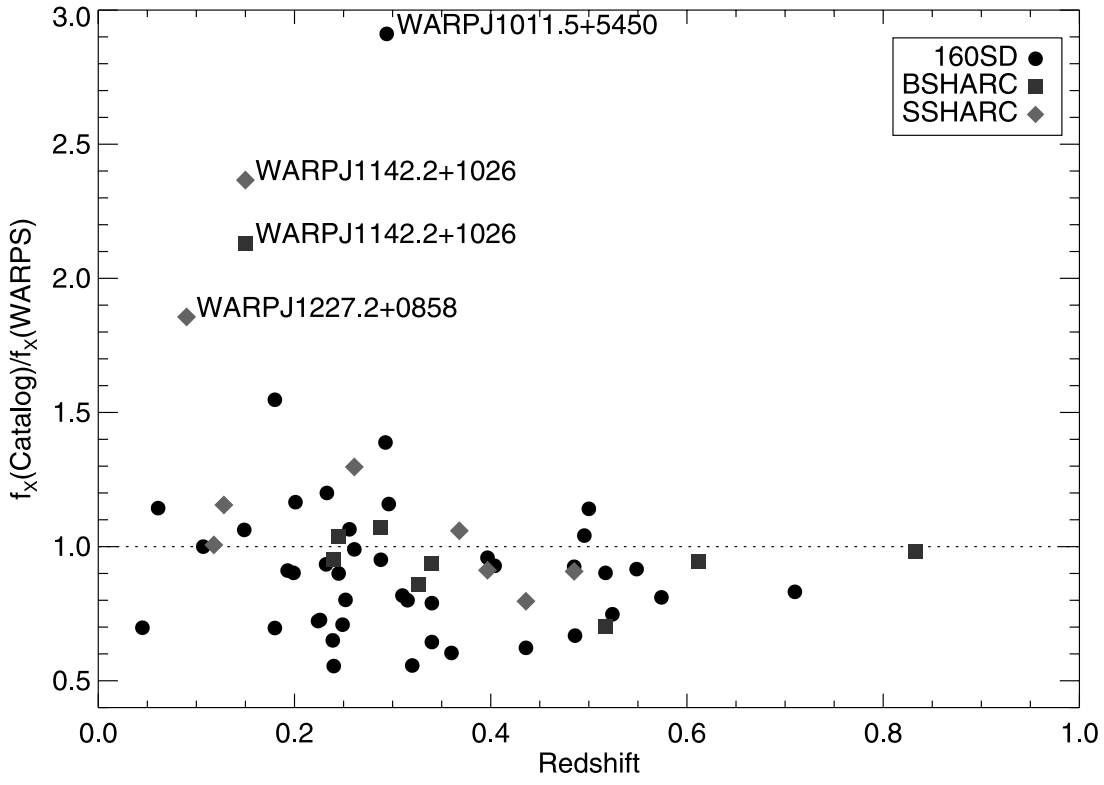

FIG. 5.—Comparison of X-ray fluxes for common clusters between WARPS-II and other X-ray cluster surveys.

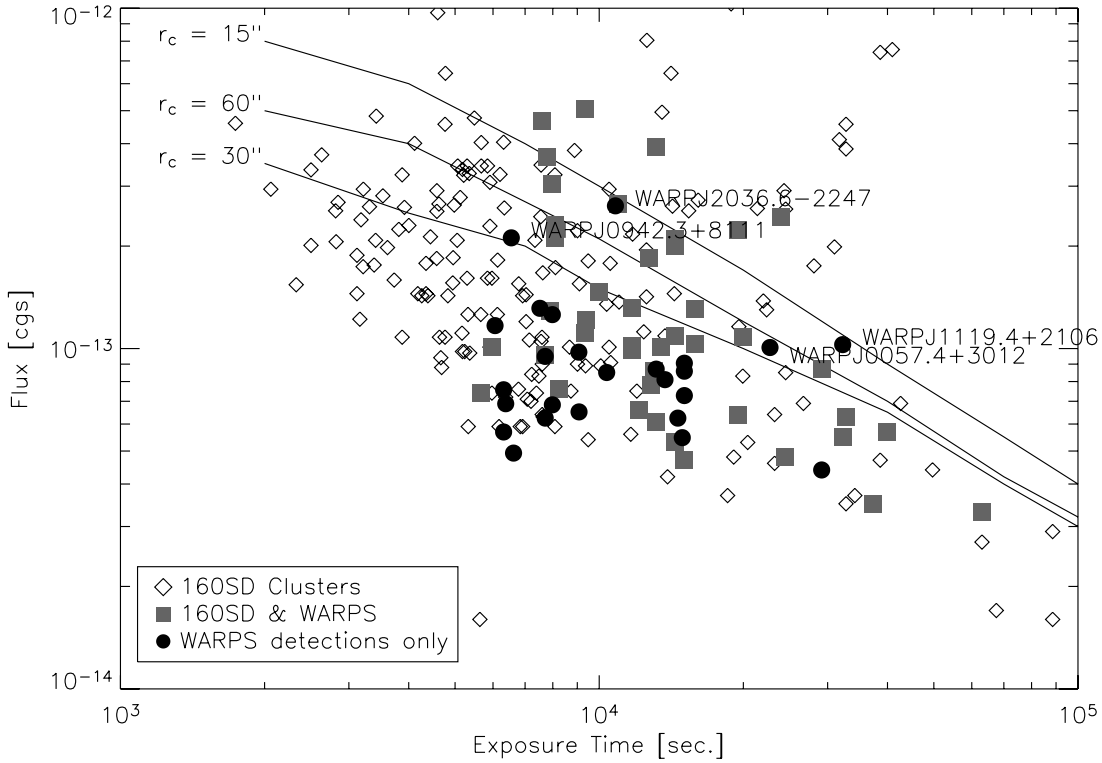

FIG. 6.—Approximate limiting flux (for 90% cluster detection probability) vs. exposure time for the 160SD survey. Limiting fluxes for three different core radii are shown. Sensitivity is best for ≈30″ and decreases for smaller and larger values. See also Fig. 6 in Vikhlinin et al. (1998). Diamonds represent clusters detected as part of the 160SD survey. Filled squares represent clusters detected in both the 160SD and WARPS surveys. Filled circles represent clusters detected only by WARPS in common *ROSAT* fields.

obtained did not seem to show a cluster. The lower 1 σ error on the 160SD flux [$(7.5 \pm 2.2) \times 10^{-14}$ ergs cm^{-2} s^{-1}] would roughly agree with our flux and put it below our flux limit.

RX J0910.6+4248 (*no. 69*).—This source has a listed flux of $(8.3 \pm 2.0) \times 10^{-13}$ ergs cm^{-2} s^{-1}, putting it only about 1 σ above our flux limit.

RX J1237.4+1141 (*no. 122*).—This source is not given a redshift in either Vikhlinin et al. (1998) or Mullis et al. (2003) due to its large angular extent. We did not detect any sources near the 160SD centroid position in our processing.

RX J1309.9+3222 (*no. 131*).—Our detection had a low flux estimate and low SNR, which is reflected in the large error in the 160SD flux [$(9.00 \pm 2.9) \times 10^{-14}$ ergs cm^{-2} s^{-1}], which puts it less than 1 σ above our flux limit.

RX J1343.4+5547 (*no. 150*).—This cluster was detected as an extended source in our processing with a flux of 1.14×10^{-13} ergs cm^{-2} s^{-1} but was manually split into two parts. The northern part has a pointlike radial profile. The southern part is extended, and we obtained two redshifts at $z = 0.068$ (consistent with the 160SD redshift). However, the estimated flux of the southern component ($\sim 6 \times 10^{-14}$ ergs cm^{-2} s^{-1}) put it below our flux limit, and no further follow-up was done.

RX J1354.8+6917 (*no. 152*).—The 160SD flux [$(6.4 \pm 1.9) \times 10^{-14}$ ergs cm^{-2} s^{-1}] is just below our flux limit. Our flux estimate was lower, and it did not pass our initial processing.

RX J1729.0+7440 (*no. 194*).—This source was detected in our initial processing and is well above our flux limit [with a flux of $(1.7 \pm 0.7) \times 10^{-13}$ ergs cm^{-2} s^{-1} in the 160SD catalog]. It is a low surface brightness source and, based on its X-ray appearance, may suffer some point-source contamination. Our follow-up imaging did not reveal any galaxies that seemed to be associated with the X-ray contours. The galaxies that seem to be at the 160SD redshift of $z = 0.213$ lie outside our X-ray contours. This source could be a misidentification by the 160SD survey.

There are 25 WARPS-II clusters in common *ROSAT* fields that are not in the 160SD catalog. Given their completeness function (Table 5 and Fig. 6 in Vikhlinin et al. 1998), most of these clusters are well below their 90% completeness threshold, which depends on the source flux, core radius, and exposure time of the *ROSAT* observation. Their sensitivity for a given flux and exposure time is best for $r_c = 30''$ and decreases at larger and smaller core radii. Figure 6 shows the limiting (90% completeness) flux for the 160SD survey for three different core radii. We have plotted WARPS clusters that were not detected by the 160SD survey.

Only four WARPS marked in Figure 6 could present issues for their completeness. However, we measure a core radius of 6.6″ for WARP J1119.4+2106 that would put in below their 90% completeness threshold. For WARP J0942.3+8111 we find a core radius of 33.4″, which would place it just at their 90% completeness threshold. The situations for other two clusters are more complicated. WARP J2036.6−2247 is a low surface brightness double cluster near the limit of our detectability, so the measured core radius is not physical. This source was not detected at all by the 160SD survey (A. Vikhlinin 2004, private communication). WARP J0057.4+3012 was detected by the 160SD survey but did not meet their selection criteria because of the low significance for being an extended object. They also find a much lower flux (3.3 ± 10^{-14} ergs cm^{-2} s^{-1}) and smaller core radius (15″) (A. Vikhlinin 2004, private communication). In spite of these

differences, there do not seem to be serious discrepancies between WARPS and the 160SD survey.

4.2. *Serendipitous High-Redshift Archival ROSAT Cluster Survey*

The Serendipitous High-Redshift Archival *ROSAT* Cluster Survey (SHARC) produced two very different samples. The Bright SHARC (BSHARC; Romer et al. 2000) contains 37 clusters with fluxes $f_x \gtrsim 3 \times 10^{-13}$ ergs cm^{-2} s^{-1} in a relatively large sky area 178.6 deg^2. The Southern SHARC Survey (SSHARC; Burke et al. 2003) contains 32 clusters but is both narrower (only 17.7 deg^2) and deeper ($f_x \gtrsim 4 \times 10^{-14}$ ergs cm^{-2} s^{-1}) than the BSHARC sample. In Paper VI, we discussed in detail the differences between our survey technique and that of the Bright SHARC survey, which used a completely automated "friends-of-friends" analysis to screen for possibly blended X-ray sources.

We find 9 clusters in common with BSHARC and 9 in common with SSHARC. For these sources, our fluxes tend to be in fair agreement (see Table 4). Our redshifts agree fairly well with SHARC redshifts, except for two cases. The BSHARC survey identified WARP J1524.6+0957 (RX J1524.6+0957) as a low-redshift group. However, we identify the actual X-ray emitter as a high-redshift cluster ($z = 0.517$). The source is also in the 160SD survey, who reach a similar conclusion to ours (for a more extensive discussion of this source, see Mullis et al. 2003). Both the BSHARC and SSHARC surveys identify WARP J1142.2+1026 (RX J1142.2+1026 or RX J1142.2+1027 in their notation) as Abell 1356 and use its literature redshift $z = 0.07$. However, the cluster region is complicated. It contains the optical clusters Abell 1354, Abell 1356, and MKW 10, and optical imaging reveals many galaxies. We find that the X-rays seem to originate from a position away from Abell 1356. Our spectroscopic follow-up finds two galaxies at $z = 0.15$ near the X-ray centroid (see § 3.2), so we believe the X-ray emission originates from a more distant cluster.

Figure 5 and Table 5 show the comparison of WARPS to SHARC fluxes. In both SHARC catalogs, WARP J1142.2+1026 has a flux higher by more than a factor of 2. Excluding this cluster lowers the average ratio of BSHARC to WARPS fluxes to 0.89, similar to the result for the 160SD survey. SSHARC contains a second cluster with much higher flux, WARP J1227.2+0858. These two clusters may be contaminated by other nearby sources in the SHARC flux measurements. Excluding both WARP J1227.2+0858 and WARP J1142.2+1026 gives a flux ratio of 1.02. This is somewhat higher than the results of 160SD or BSHARC and confirms the trend noted in Burke et al. (2003) and Mullis et al. (2003) for SSHARC to give higher fluxes compared to 160SD.

In the 159 and 14 common fields with BSHARC and SSHARC, respectively, we find no SHARC clusters that are not in WARPS-II (except for those out of the 3′–15′ area we covered in the field). We find 83 clusters in common fields that the BSHARC survey does not. Fourteen of these are above their count rate limit of 0.01163 counts s^{-1}. See Paper VI for a discussion of the possible shortcomings of the BSHARC methodology. We find three clusters that the SSHARC survey does not. Two of these have $z < 0.2$, which SSHARC is not designed to accurately catalog (Burke et al. 2003). The remaining source (WARP J1002.6−0808) has a redshift of $z = 0.5240$ and flux 1.15×10^{-13} ergs cm^{-2} s^{-1}. It is listed in the SSHARC catalog of extended sources as RX J1002.6−0809, but they apparently concluded that their optical follow-up did not support the existence of a cluster. This cluster is also in the 160SD catalog (as RX J1002.6−0808 or no. 83), and Mullis et al. (2003) note that it is also in the RDCS sample. Therefore, we are fairly confident in our identification of this source as a cluster.

4.3. *ROSAT International X-Ray/Optical Survey*

The *ROSAT* International X-ray/Optical Survey (RIXOS; Mason et al. 2000) attempted to identify all X-ray sources (not just clusters) in 64 *ROSAT* fields (15.77 deg^2) down to 3×10^{14} ergs cm^{-2} s^{-1}, although their search algorithm was optimized for point sources. There is a significant overlap between RIXOS and WARPS-II. Of the 64 *ROSAT* fields included in RIXOS, 55 are shared by the WARPS-II sample.

There are 14 WARPS-II clusters that are also listed as clusters in the RIXOS survey. Three additional WARPS clusters were also detected by RIXOS but classified as nonclusters. Two of these clusters were listed as "unidentified," and one (WARP J1331.5+1108) is classified as an emission line galaxy (ELG). Overall, WARPS and RIXOS redshift measurements agree fairly well. However, the flux measurements do not. RIXOS gives two flux measurements for each source. The first is derived by converting the count rate to flux assuming a spectral slope $\alpha = -1$. This flux used to determine membership in their catalog. The second is derived from the best-fitting slope to the *ROSAT* PSPC spectrum. We find that both measures are significantly lower than the WARPS fluxes with a mean and standard deviation of $f_x(\mathrm{RIXOS})/f_x(\mathrm{WARPS}) = 0.72 \pm 0.31$ for the $\alpha = -1$ fluxes and $f_x(\mathrm{RIXOS})/f_x(\mathrm{WARPS}) = 0.40 \pm 0.19$ for the other (see Table 5). This is quite likely due to the lack of a correction for extended sources. For the rest of this section, we will assume the $\alpha = -1$ fluxes when comparing to RIXOS.

In the common area of the shared fields, there are two clusters in RIXOS that are not in WARPS. The RIXOS flux for RX J141916.7+541417 (4.0×10^{-14} ergs cm^{-2} s^{-1}) puts it well below our flux limit even with the difference in flux measurements. However, the RIXOS identification is not very secure as they list only one uncertain redshift for this cluster. We detected this source in our processing but classified it as a point source. Due to the small extent (0.04) of the X-ray source, the X-ray emission unlikely to due to a cluster.

The situation for the second RIXOS cluster, RX J083918.7+361855, is more complicated. The RIXOS team measured $z = 0.335$ for the galaxy within the X-ray error circle and for a second galaxy nearby. Having two galaxies at the same redshift and several more galaxies apparent in the optical images, they identified the X-ray source as a cluster (F. J. Carrera 2004, private communication). The flux of the source (3.3×10^{-13} ergs cm^{-2} s^{-1}) is well above our flux limit, and we did not detect the source as extended in our processing. We classified it as a point source and did not follow it up. After discussion with the RIXOS group and examining their spectra, we obtained our own spectrum of the galaxy nearest the X-ray position that resembles that of a BL Lac object. The X-ray position is also coincident with a radio source. The optical spectrum, X-ray pointlike appearance, and radio flux are all consistent with a BL-Lac object. We feel that this may be a case of an AGN in or behind a poor cluster of galaxies with most of the X-ray flux coming from the point source. Note that this *ROSAT* field is also in the 160SD and BSHARC surveys, who likewise did not detect this source as a cluster.

In the 55 common *ROSAT* fields, we find 11 clusters that are not in the RIXOS sample but are above the RIXOS flux limit. All of these clusters have $z > 0.25$. Incompleteness due to inaccurate

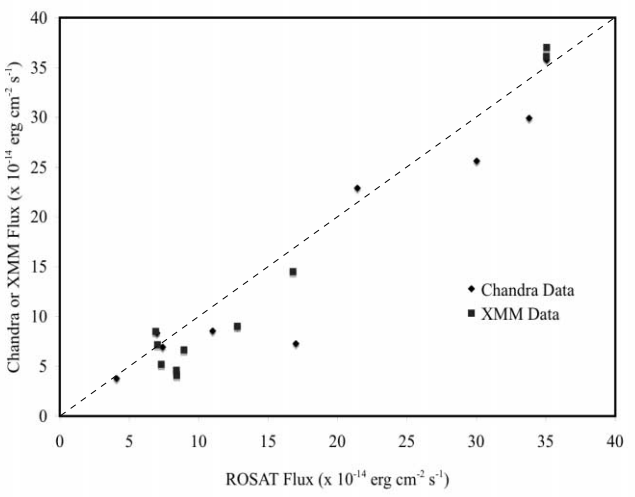

FIG. 7.—Comparison of the fluxes measured by *ROSAT*, *Chandra* and *XMM-Newton* for WARPS clusters. Squares represent clusters observed by *XMM-Newton*, and diamonds represent clusters observed by *Chandra*. Where available, we show both ratios for clusters that were observed by both satellites. The dashed line shows a ratio of 1. As can be seen, there is a slight tendency for the *ROSAT*-measured fluxes to be higher; this is due to contamination by point sources. See § 4.4.

fluxes for extended sources in the RIXOS survey of Castander et al. (1995) has been noted previously (Burke et al. 1997; Jones et al. 1998; Rosati et al. 2002).

4.4. *Chandra and XMM-Newton Observations*

A significant number of WARPS clusters have been observed by X-ray satellites with better sensitivity and angular resolution (i.e., *Chandra*, *XMM-Newton*). We have already discussed in § 3 the details of these observations for individual sources. In Figure 7, we compare the *ROSAT* fluxes (as measured in WARPS) to those measured by either *Chandra* or *XMM-Newton* (Maughan et al. 2006b, 2008). We include in Figure 7 both objects that are included in this sample (WARPS-II, 14 objects) as well as WARPS-I (4 objects; see Paper VI). We do this for the sake of completeness, as the WARPS-I survey technique was very similar to ours and the flux measurements were generated using essentially identical methods. Where flux measurements were available for both *Chandra* and *XMM-Newton*, we have included both in Figure 7. As can be seen, Figure 7 shows some tendency for the *ROSAT* flux measurements to be slightly higher than those found by *Chandra* or *XMM-Newton*. We find flux ratios of $F(ROSAT)/F(Chandra) = 1.23 \pm 0.42$ and $F(ROSAT)/F(XMM\text{-}Newton) = 1.29 \pm 0.40$. However, these numbers decline significantly [to $F(ROSAT)/F(Chandra) = 1.10 \pm 0.18$ and $F(ROSAT)/F(Chandra) = 1.13 \pm 0.24$] when the three most extreme clusters (discussed below) are excluded. The most likely reason for this difference of typically ~10%–20% lies in the presence of point sources—either serendipitous or associated with cluster galaxies—within the X-ray emission contours (and hence the VTP source detection region) of the cluster. Indeed, as noted by Maughan et al. (2008), X-ray–luminous clusters typically have up to 10 and sometimes more point sources located within R_500, and the WARPS clusters are no exception to this rule (indeed, their numbers of point sources are typical). There are three clusters where we observe considerably higher ratios of *ROSAT* to *Chandra* or *XMM-Newton* flux: namely, WARP J0035.9+8513, WARP J0216.5+1747, and WARP J1559.1+6353. In each case this is because of the X-ray point sources in the field account for a larger percentage of the *ROSAT* flux.

5. SUMMARY

We have presented the galaxy cluster catalog and finder charts from the second, larger phase of the Wide Angle *ROSAT* Pointed Survey (WARPS), an X-ray selected survey for high-redshift galaxy clusters. The WARPS-II sample contains 125 clusters in a sky area of 56.7 deg^2 and a statistically complete sample of 102 clusters above a uniform flux limit of 6.5×10^{-14} ergs cm^{-2} s^{-1} (0.5–2.0 keV). Together with the WARPS-I sample, WARPS has found a total of 159 clusters in 72.9 deg^2 with a statistical subsample of 124 clusters. We have spectroscopic redshifts for nearly every cluster, with only a few with dubious or unknown redshifts. The clusters range in redshift from $z = 0.029$ to $z = 0.92$ with a median redshift of $z = 0.29$ and span almost 4 orders of magnitude in X-ray luminosity.

We compared our redshifts, fluxes, and detection methods to other published cluster surveys (160SD, SHARC, and RIXOS) that are based on *ROSAT* PSPC data. We have 157 *ROSAT* fields and 44 clusters in common with the 160SD survey. Our measured fluxes typically agree fairly well with the 160SD fluxes, although ours are systematically higher by about 10% on average with a 20% scatter. While there are some differences in detections, i.e., clusters found in one survey but not another, these discrepancies can mostly be ascribed to differences in flux measurements affecting sources near flux or completeness limits. We have a much smaller overlap in terms of number of sources with the two SHARC surveys, BSHARC and SSHARC, with only nine clusters in common between WARPS-II and each survey. There are typically no significant differences in fluxes. There are some discrepancies in the detection or nature of individual sources, but the comparison reveals no shortcomings in WARPS detection methods. We find that the fluxes of clusters in the RIXOS survey are well underestimated by comparing the 14 in common between the surveys. Again, no problems with WARPS detections methods are revealed.

We acknowledge useful discussions with Alexey Vikhlinin and Francisco J. Carrera, and data contributions from C. Mullis. The WARPS team acknowledges the long-term support of many different time allocation committees, including those at Kitt Peak National Observatory, Cerro Tololo Inter-American Observatory, and the University of Hawaii, for the observations detailed in this paper. E. S. P. and H. E. acknowledge support from HST program GO-9033. H. E. acknowledges support from NASA grant NAG 5-10085. During this work, B. J. M. was supported by a *Chandra* Postdoctoral Fellowship, award PF4-50034. B. J. M., H. E., and L. R. J. gratefully acknowledge support from *Chandra* grant GO0-1071A and NASA grant NNG 06-GD78G. Part of the observations used in this paper were obtained at the MDM Observatory on Kitt Peak. Some of the data presented herein were obtained at the W. M. Keck Observatory, which is operated as a scientific partnership among the California Institute of Technology, the University of California, and the National Aeronautics and Space Administration. The Keck Observatory was made possible by the generous financial support of the W. M. Keck Foundation. This research has made use of data obtained through the High Energy Astrophysics Science Archive Research Center Online Service, provided by the NASA Goddard Space Flight Center. This research has made use of the NASA/IPAC Extragalactic Database (NED), which is operated by the Jet Propulsion Laboratory, California Institute of Technology, under contract with the National Aeronautics and Space Administration.

REFERENCES

Arnaud, M., et al. 2002, A&A, 390, 27
Böhringer, H., et al. 2000, ApJS, 129, 435
Burke, D. J., Collins, C. A., Sharples, R. M., Romer, A. K., Holden, B. P., & Nichol, R. C. 1997, ApJ, 488, L83
Burke, D. J., Collins, C. A., Sharples, R. M., Romer, A. K., & Nichol, R. C. 2003, MNRAS, 341, 1093
Cagnoni, I., Elvis, M., Kim, D.-W., Mazzotta, P., Huang, J.-S., & Celotti, A. 2001, ApJ, 560, 86
Castander, F. J., Bower, R. G., Ellis, R. S., Aragon-Salamanca, A., Mason, K. O., Hasinger, G., McMahon, R. G., Carrera, F. J., Mittaz, J. P. D., Perez-Fournon, I., & Lehto, H. J. 1995, Nature, 377, 39
Della Ceca, R., Scaramella, R., Gioia, I. M., Rosati, P., Fiore, F., & Squires, G. 2000, A&A, 353, 498
Demarco,R. 2005, A&A, 432, 381
Dickey, J. M., & Lockman, F. J. 1990, ARA&A, 28, 215
Donahue, M., et al. 2001, ApJ, 552, L93
Ebeling, H. 1993, Ph.D. thesis, Ludwig-Maximilians-Universität München
Ebeling, H., Edge, A. C., Böhringer, H., Allen, S. W., Crawford, C. S., Fabian, A. C., Voges, W., & Huchra, J. P. 1998, MNRAS, 301, 881
Ebeling, H., Jones, L. R., Fairley, B. W., Perlman, E., Scharf, C., & Horner, D. 2001, ApJ, 548, L23 (Paper V)
Ebeling, H., Jones, L. R., Scharf, C. A., Perlman, E., Horner, D., Wegner, G., Malkan, M., Fairley, B.,, & Mullis, C. R. 2000, ApJ, 534, 133 (Paper III)
Ebeling, H., & Wiedenmann, G. 1993, Phys. Rev. E, 47, 704
Ellis, S. C., & Jones, L. R. 2004, MNRAS, 348, 165
Fairley, B. W., Jones, L. R., Scharf, C., Ebeling, H., Perlman, E., Horner, D., Wegner, G., & Malkan, M. 2000, MNRAS, 315, 669 (Paper IV)
Holden, B. P., Stanford, S. A., Squires, G. K., Rosati, P., Tozzi, P., Eisenhardt, P., & Spinrad, H. 2002, AJ, 124, 33
Holden, B. P., et al. 2001, AJ, 122, 629
———. 2005, ApJ, 626, 809
Huo, Z.-Y., Xue, S.-J., Xu, H., Squires, G., & Rosati, P. 2004, AJ, 127, 1263
Jee, M. J., White, R. L, Benítez, N., Ford, H. C., Blakeslee, J. P., Rosati, P., Demarco, R., & Illingworth, G. D. 2005, ApJ, 618, 46
Jones, L. R., Ponman, T. J., Horton, A., Babul, A., Ebeling, H., & Burke, D. J. 2003, MNRAS, 343, 627
Jones, L. R., Scharf, C., Ebeling, H., Perlman, E., Wegner, G., Malkan, M., & Horner, D. 1998, ApJ, 495, 100 (Paper II)
Jorgensen, I., Bergmann, M., Davies, R., Barr, J., Takamiya, M., & Crampton, D. 2005, AJ, 129, 1249
Joy, M., et al. 2001, ApJ, 551, L1
Lewis, A. D., Stocke, J. T., Ellingson, E., & Gaidos, E. J. 2002, ApJ, 566, 744
Mason, K. O., et al. 2000, MNRAS, 311, 456
Maughan, B. J., Ellis, S. C., Jones, L. R., Mason, K. O., Córdova, F. A., Priedhorsky, W. 2006a, ApJ, 640, 219
Maughan, B. J., Jones, L. R., Ebeling, H., Perlman, E., Rosati, P., Frye, C., & Mullis, C. R. 2003, ApJ, 587, 589
Maughan, B. J., Jones, L. R., Ebeling, H., & Scharf, C. 2004a, MNRAS, 351, 1193
———. 2006b, MNRAS, 365, 509
Maughan, B. J. Jones, C., Forman, W., & van Speybroeck, L. 2008, ApJS, 174, 117
Maughan, B. J., Jones, C., Jones, L. R., & van Speybroeck, L. 2007, ApJ, 659, 1125
Maughan, B. J., Jones, L. R., Lumb, D., Ebeling, H., & Gondoin, P. 2004b, MNRAS, 354, 1
Mullis, C. R., McNamara, B. R., Quintana, H., Vikhlinin, A., Henry, J. P., Gioia, I. M., Hornstrup, A., Forman, W., & Jones, C. 2003, ApJ, 594, 154
Perlman, E. S., Horner, D. J., Jones, L. R., Scharf, C. A., Ebeling, H., Wegner, G., & Malkan, M. 2002, ApJS, 140, 265 (Paper VI)
Postman, M., et al. 2005, ApJ, 623, 721
Romer, A. K., Nichol, R. C., Holden, B. P., Ulmer, M. P., Pildis, R. A., Merrelli, A. J., Adami, C., Burke, D. J., Collins, C. A., Metevier, A. J., Kron, R. G., & Commons, K. 2000, ApJS, 126, 209
Rosati, P., Borgani, S., & Norman, C. 2002, ARA&A, 40, 539
Rosati, P., Della Ceca, R., Norman, C., & Giacconi, R. 1998, ApJ, 492, L21
Rosati, P., Stanford, S. A., Eisenhardt, P. R., Elston, R., Spinrad, H., Stern, D., & Dey, A. 1999, AJ, 118, 76
Scharf, C. 2002, ApJ, 572, 157
Scharf, C. A., Jones, L. R., Ebeling, H., Perlman, E., Malkan, M., & Wegner, G. 1997, ApJ, 477, 79 (Paper I)
Vikhlinin, A., McNamara, B. R., Forman, W., Jones, C., Quintana, H., & Hornstrup, A. 1998, ApJ, 502, 558
White, D. A., Jones, C., & Forman, W. 1997, MNRAS, 292, 419